ABSTRACT

Title of Document: HEAT FLUX-BASED EMISSIVITY MEASUREMENT.

Joseph Currano, Master of Science in Mechanical Engineering, 2007

Directed By: Associate Professor, Dr. Jungho Kim, Mechanical Engineering

A method for measuring the emissivity of a surface using heat flux sensors is described. The emissivity is calculated by directly measuring the heat flux passing through the surface using a heat flux sensor. Unlike calorimetric techniques, it does not require accounting for parasitic heat losses or knowing the temperature history of the sample. This technique allows emissivity measurements of newly developed variable emissivity surfaces, including electrostatic devices which cannot be directly measured using optical techniques. It can measure both passive and active thermal control coatings, and can evaluate many surfaces on the same substrate simultaneously. An experimental setup is detailed and results are presented for emissivity measurements of both active and passive surfaces using commercially available heat flux sensors. Errors are estimated for these measurements. A space-based experiment is also described and results of pre-flight testing are presented.

HEAT FLUX-BASED EMISSIVITY MEASUREMENT

By

Joseph A. Currano

Thesis submitted to the Faculty of the Graduate School of the
University of Maryland, College Park, in partial fulfillment
of the requirements for the degree of
Master of Science in
Mechanical Engineering
2007

Advisory Committee:
Professor Jungho Kim, Chair
Professor Gregory Jackson
Professor Bao Yang

Acknowledgements

This research was performed under the direction of Advanced Thermal and Environmental Concepts (ATEC), Inc., with the support of the Air Force SBIR Phase II Contract FA8650-05-C-5045, administered by the SBIR Program Office at the Air Force Research Laboratory, Wright-Patterson Air Force Base. I would like to thank John Lawler of ATEC and Saeed Moghaddam, formerly of ATEC, as well as Dr. Jungho Kim, for all of their guidance in this research and in my education.

Table Of Contents

List of Tables

List of Figures

Nomenclature

A – area [m^2]
d – distance [m]
F – radiation view factor
k_0 – thermal conductivity at atmospheric pressure [W/m-K]
k_e – effective thermal conductivity [W/m-K]
l – characteristic length for Knudsen number [m]
T – temperature [K]
P – pressure [Pa]
$\dot{q}''$ – heat flux [W/m^2]
$\dot{q}$ – heat transfer rate [W]
S – conduction shape factor
V – voltage [V]

Greek Symbols

α - absorptivity
ε - emissivity (total hemispherical)
λ - transmissivity
ρ - reflectivity
σ - Stefan-Boltzmann constant, 5.67×10^{-8} $W/m^2\text{-}K^4$
τ - transmissivity

Subscripts

1-2 – From surface 1 to surface 2
S – substrate or sample surface
∞ - far-field

Chapter 1: Introduction

The temperature of a satellite and its components must remain within certain limits to avoid failure. Since radiation is the primary means of heat transfer in space, the radiation properties of surface materials are an important field of spacecraft thermal control. The temperature of a satellite is determined by the heat generated internally (e.g., by electronic components), heat received from the sun and other sources of radiation, and heat emitted from the satellite to space. For any surface, the heat received and emitted by radiation depends on the optical properties of the surface, namely absorptivity, emissivity, reflectivity, transmissivity.

Every surface at a temperature above 0 K emits thermal energy in the form of electromagnetic waves, which is termed thermal radiation. Emissivity is the ratio of energy emitted by a surface to the theoretical limit (blackbody radiation) at the same temperature. Absorptivity is the fraction of incident radiation which is absorbed by a surface. Reflectivity and transmissivity are the fractions of incident radiation reflected and transmitted through the surface, respectively. The absorptivity, reflectivity, and transmissivity of a surface must total 1. Thus, the reflectivity and absorptivity are related, and for opaque surfaces (zero transmissivity), the energy received and emitted by radiation is governed entirely by the emissivity and the absorptivity of the surface. Thus, to keep the temperature of a satellite at an operational level, careful design of the outer surfaces with respect to absorptivity and emissivity is critical. Moreover, accurate measurement of these properties is necessary to assess new materials and structures for satellite thermal control.

Recent developments in variable emissivity surfaces and the need for testing them in space environments have generated a demand for emissivity measurement equipment that is lighter, more efficient, and less complex than conventional emissivity measurement techniques. Unlike traditional constant emissivity surfaces such as paints and films, the new variable emissivity surfaces are more complex in structure and performance. Variable emissivity surfaces can be based on different concepts such as changing the optical properties of the surface material itself or modifying the surface structurally to alter its radiation heat transfer performance. Polymer-based materials [1] and inorganic thin films [2, 3] can have variable optical properties, as in electrochromic devices. Two mechanically active coatings under development are electrostatic devices, [4, 5] also called Electrostatic Switched Radiators (ESRs), and MEMS louvers.[6] An ESR operates in vacuum by opening and closing a gap between two surface layers via electrostatic forces, with the gap hindering heat transfer through the surface layers. The effective emissivity is controlled by making the base layer a low emissivity surface and the top layer a high emissivity surface. With voltage applied, the top layer is attracted to the base layer by the electrostatic force, allowing heat to conduct into the top layer, so the effective emissivity is approximately that of the top layer. In the deactivated state, the gap between the layers prevents conduction. Heat must radiate from the base layer to the top layer before radiating outward, so the effective emissivity is closer to that of the base layer.[4, 5] MEMS louvers are microfabricated versions of the larger scale louvers that were developed earlier for spacecraft, in which vanes are opened and closed to vary the effective emissivity of a surface.[6] The acceptance of these active thermal control systems requires a demonstration of their performance in a relevant space environment.

The most common methods used for measuring the emissivity of a surface are based on calorimetric and optical methods. Calorimetry involves measuring the power delivered to the test sample as well as the temperatures of the emitting surface (the sample) and the surroundings in a vacuum over time.[8, 9] An energy balance is then used to determine the emissivity. The sample must be well insulated on the sides and back, and parasitic heat losses must be accounted for to accurately determine the heat transfer through the sample surface. Optical techniques involve illuminating a sample with infrared energy and measuring the percentage of energy reflected from the surface.[10] The absorptance is calculated from the reflectance and used to calculate normal emittance by Kirchhoff's Law. The optical method is generally less labor-intensive than the calorimetric method, but the measurements must be repeated at all angles and then numerically integrated to accurately obtain the total hemispherical emissivity. In many cases this is not practiced and the normal emissivity is considered as an approximation of the hemispherical emissivity. Although the complexity of measuring the emissivity of spatially and temporally variable emissivity surfaces can be overcome using sophisticated testing equipment designed for conventional emissivity measurement techniques in a lab environment, the application of such systems in space is associated with a significant weight, energy consumption, and data volume.

A heat-flux based (HFB) emissivity measurement method has been developed that employs commercially available heat flux sensors. In the HFB method, the heat flux through the emitting surface is directly measured using one or more (depending on the required spatial resolution) heat flux sensors placed between the sample surface and the

substrate on which the surface is installed. This allows emissivity measurement of surfaces as they operate in space or in a thermal vacuum chamber.

The low thermal capacitance of the available heat flux sensors can provide good temporal resolution of the heat flux. The small size of the sensors can provide the necessary spatial resolution to resolve the performance of a spatially variable emissivity surface if desired. Since the heat flux through individual samples is measured, the HFB method can be used to evaluate multiple surfaces with different emissivities simultaneously on the same substrate.

The HFB method measures hemispherical emissivity without the need for careful thermal insulation of the substrate or multiple optical measurements at different angles. The HFB method can measure spatial variations of emissivity without the complexity and labor-intensity of the optical method. Furthermore, the HFB method provides real-time measurement of the surface emissivity through direct measurement of heat flow through the emitting surface, allowing evaluation of changes in surface properties over time.

The HFB method requires minimal data measurement and processing. The heat flux passed through the surface (measured by the heat flux sensor), the surface temperature, and the enclosure temperature are the only information required to calculate the surface emissivity, as long as radiation is the only significant mode of heat transfer from the surface to the enclosure. This method requires neither the temperature history nor thermal insulation of the substrate on which the variable emissivity surface is installed. In addition to its simplicity and significantly reduced data volume, the HFB emissivity measurement method eliminates the need for heaters and their power measurement equipment, control system, and heating energy that is at a premium in any

space mission. The HFB method can measure the emissivity of an active surface such as an ESR while it is operating as part of a space vehicle's thermal control system.

The objectives of this work are to demonstrate the capability of the HFB method in measuring the emissivity of passive and active surfaces, to use the HFB technique for studying the performance of an ESR, and to develop an experiment for testing the HFB technique in space. The passive surfaces used in this study are: standard black spray paint, black and white emissivity control paints, a carbon-fiber appliqué, and a gold-coated tape. For the active surfaces, several models of the ESR developed by Sensortex, Inc., were tested.

A space experiment that incorporates the HFB emissivity measurement method was also developed. A module incorporating four passive and two active surfaces, with all the necessary electronics, was built for testing on the International Space Station (ISS) under the Materials International Space Station Experiments (MISSE-6) mission. This module was tested in the laboratory before being incorporated into MISSE-6, which is expected to be deployed for six months attached to a truss of the ISS beginning April, 2008.

Chapter 2: Existing Methods of Measuring Emissivity

Calorimetric Techniques

Calorimetry involves performing an energy balance on a sample surface radiating out to a blackbody. Two calorimetric methods are used to determine the emissivity of a surface: a steady thermal balance method, and transient calorimetry.[7]

Measurement of emissivity by a steady thermal balance method involves measuring the power delivered to the test sample as well as the temperatures of the emitting surface (the sample) and the surroundings in a vacuum over time.[8, 9] The substrate temperature is allowed to come to equilibrium with a constant power applied to a heater in thermal contact with the sample. An energy balance is then used to determine the emissivity through the Stefan-Boltzmann law of radiation. To do this, an enclosure of uniform temperature capable of holding high vacuum is used to act as a blackbody, simulating radiation to deep space. The sample must be well insulated on the sides and back using a heat shield, and parasitic heat losses must be accounted for to accurately determine the heat transfer through the sample surface. This means that only one sample may be measured at a time. Furthermore, it requires the temperatures of the sample and heat shield to be precisely controlled and to reach steady state before emissivity data is obtained. Thus, data is taken for a single temperature during each test run, and the test must be performed at various temperatures to generate a curve of emissivity versus temperature.

The transient calorimetric method uses a similar setup but instead of relying on an equilibrium state, the sample is applied to a substrate of known specific heat capacity (e.g., aluminum) and the assembly is allowed to cool down in the chamber. The

emissivity can be calculated from the specific heat, the total area of the sample, and the cooling rate. Parasitic heat losses should also be accounted for as they can affect the measurement. The time required for cooling can be substantial, even up to several weeks for a low emissivity sample.[7] Transient calorimetry is the most time-intensive method. Calorimetric methods cannot measure sudden changes in the emissivity of an active thermal control surface, but can only measure the emissivity for each state individually.

Optical Techniques

Optical techniques of measuring emissivity involve illuminating a sample with infrared energy and measuring the percentage of energy reflected from the surface, using a reflectometer or spectrophotometer.[10] The absorptance (α) is calculated from the reflectance (ρ) by a radiative energy balance:

$$\alpha + \tau + \rho = 1 \tag{1}$$

where in the case of an opaque surface, the transmissivity τ =0. If the surface is not opaque, the percentage of transmitted energy may also be measured. The absorptance is then used to calculate normal emittance by Kirchhoff's Law, which states that when emission and irradiation are of the same spectrum, $\varepsilon = \alpha$.[8] The optical method is generally less labor-intensive than the calorimetric method, but the measurements must be repeated at all angles and then numerically integrated to obtain the true total hemispherical emissivity. In many cases this is not practiced and the normal emissivity is used to approximate the hemispherical emissivity, sometimes using a conversion formula depending on the type of material.

This method is ineffective when evaluating certain active coatings. For instance, an electrostatic switched radiator (ESR) developed by Sensortex, Inc., relies on the

physical relaxation of a high-emissivity membrane to switch the mode of heat transfer from conduction to radiation, decreasing the heat transfer from a satellite to outer space. This causes a change in effective emissivity, but because the membrane's optical properties do not change, an optical system cannot detect this. This will be discussed further in a later section.

Chapter 3: Heat Flux-Based Measurement Method

In the heat flux-based method, a heat flux sensor is installed between the surface whose emissivity is being measured and a high conductivity substrate. Figure 1 shows a schematic of this configuration. The test substrate is placed inside a thermal vacuum chamber whose inside walls are coated with a flat black paint. The chamber is immersed in liquid nitrogen (-195°C) to simulate radiation to deep space.

The heat emitted from the surface passes through the heat flux sensor so it is measured directly. Knowing the heat flux emitted, the total hemispherical emissivity of the surface can be calculated using the Stefan-Boltzmann law of radiation:

$$\varepsilon = \frac{\dot{q}''}{\sigma\left(T_S^4 - T_\infty^4\right)} \tag{2}$$

In this equation, q'' is the heat flux per unit area (W/m^2), which is the quantity measured by the heat flux sensor. The temperature of the surface, T_S, is approximated by the temperature of the substrate. Theoretically, the direct measurement of the heat flux through the gauge makes parasitic heat loss/gain irrelevant to the measurement of emissivity, since any parasitic heat paths simply change the surface temperature, which is included in the calculation.

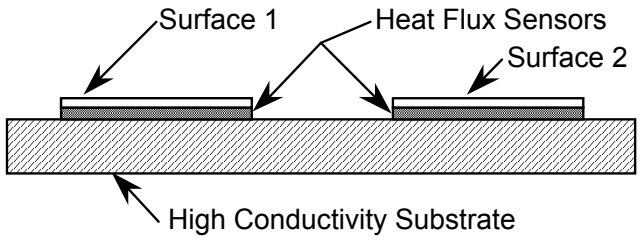

Figure 1. Schematic showing the arrangement of heat flux sensors with respect to the emitting surface.

The fact that the heat flux is measured directly should also make it possible to measure absorptivity (from the sun or other incident radiation) for a coating, since the sensor will simply give a negative heat flux reading.

Advantages of Heat Flux-Based Technique

The heat flux-based technique has several advantages over calorimetry and optical measurements. It is a relatively simple technique because it measures directly the heat flux through the sample, which is the quantity of interest in thermal management of satellites and does not require knowledge of the sample's temperature history. It is not difficult to implement using space-qualified hardware, as heat flux sensors are already used in space applications. It can be used to measure changes in emissivity of active structures.

Unlike calorimetry, the heat flux-based technique does not require elimination of parasitic heat losses from the substrate, since all that is needed for determination of the emissivity is the current temperature and the heat flux sensor reading. While the measurements must be made in vacuum, heat losses through the sides and back of the substrate, or through the structure used to support the sample, do not affect the measurement. This further allows measurements to be performed on several samples on the same substrate simultaneously.

Because the heat flux-based technique uses a direct heat flux measurement rather than an energy balance, parasitic heat losses need not be accounted for and measurements can be performed more quickly than with calorimetry, and over a range of temperatures in one test. In calorimetry, tests are performed for individual temperatures, whereas the heat flux-based technique can be used to measure the emissivity as the temperature of the

sample varies over a wide range, generating an emissivity versus temperature curve in one test. This results in much lower data volume, which is a significant advantage especially for testing in space missions where data storage is costly.

The heat flux-based technique can also measure sudden changes in the emissivity of active surfaces, since steady-state conditions are not needed. In the case of optically controlled surfaces (e.g., electrochromics), an optical measurement for each state might suffice. However, mechanically controlled structures like the Sensortex ESR cannot be evaluated by optical measurements, and calorimetry would involve two separate tests over long periods of time to ensure each state obtained steady conditions. Moreover, calorimetry is unsuitable for measuring transient effects in active emissivity structures.

The heat flux-based technique measures emissivity over all wavelengths and all angles (total hemispherical emissivity) in a single test, which is not the case with optical techniques. Some optical instruments cover a broad range of wavelengths (for example, the SOC-400T made by Surface Optics Corporation covers the range of 2 to 25 μm [10]), eliminating the need for multiple wavelength measurements, but they can only take measurements one angle at a time. Some optical systems are programmed to obtain measurements over many angles and integrate to obtain a value for hemispherical emissivity, but this is done at a cost of much more complex equipment. Often, normal reflectivity is the measurement taken, calculating the normal emissivity, which is used as an approximation for hemispherical emissivity. This approximation is more or less valid depending on the surface characteristics. Shiny surfaces generally exhibit more angular characteristics than dull surfaces.

A further benefit of the heat flux-based technique is the simplicity of incorporation into space-based measurements, where the environmental effects on thermal control coatings can be studied. Unlike optical reflectometers, the heat flux-based system can take measurements of a surface while it is radiating to and receiving radiation from space. Calorimeters have been flown in space successfully;[11] however, they are associated with high data volume and extensive instrumentation, which can be avoided by using the heat flux-based technique.

Heat Flux Sensors

The heat flux sensors used in this research are commercially available from RdF Corporation and Vatell Corporation. The heat flux sensors operate on the principle that heat passing through a passive film, which acts as a thermal barrier, creates a small temperature difference across the film. Two thermocouple junctions in series with this thermal barrier between them creates a voltage output proportional to the heat flux through the film. A heat flux sensor is composed of many of these thermocouple pairs in series to create a thermopile, amplifying the signal to provide a more easily measured output voltage. This output voltage is converted to heat flux using a calibration factor provided by the manufacturer.

The heat flux sensors from RdF used in this research are 0.178 mm (0.007 in) thick while the Vatell sensors are 0.25 mm thick (model BF04) and 0.20 mm thick (model BF07). The RdF sensors (Figure 2) are composed of a thin foil-type thermopile bonded to both sides of a Kapton film. Each side is covered by another layer of film to protect the thermopiles. The Vatell sensors (Figure 3) are similar in construction but use a fiberglass film which is more rigid. The small RdF sensors are 0.47 in x 1.8 in (11.9 mm x 45.7

mm) with a 0.47 in x 1.0 in (11.9 mm x 25.4 mm) sensing area, and both Vatell sensors are 2.5 cm x 2.5 cm (1 in x 1 in). Both the small RdF models and the two Vatell models were used for passive coatings. The difference between the two Vatell sensors is that the BF04 has a higher sensitivity. Larger, 2 in x 2 in (50.8 mm x 50.8 mm) RdF sensors were custom made for testing the active coatings.

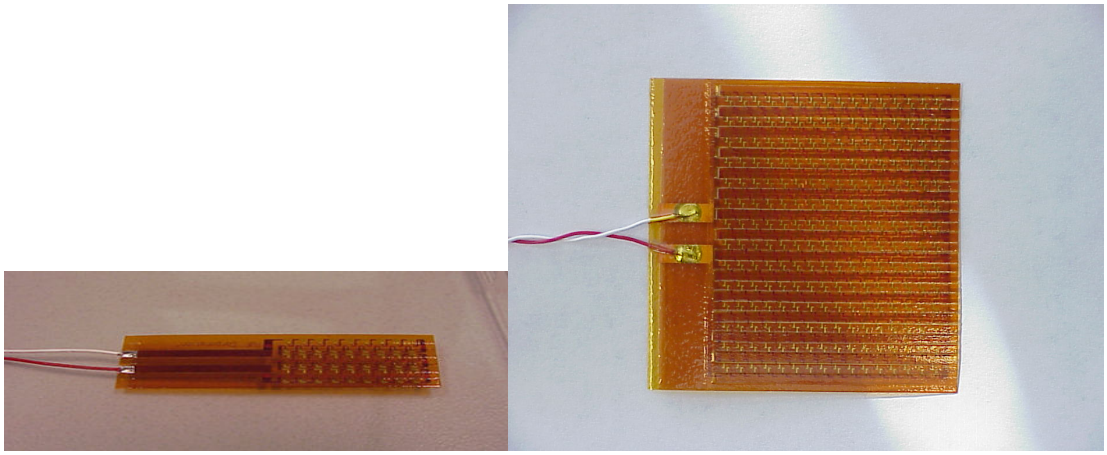

(a) (b)

Figure 2. Photographs of two RdF heat flux sensors: a) Model 27160. b) 2 in x 2 in custom-made sensor.

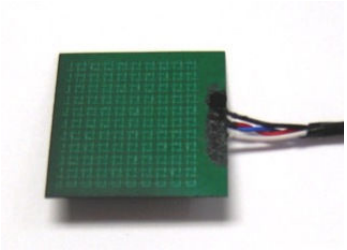

Figure 3. Vatell heat flux sensor, Model BF04.

Emissivity calculation

To obtain the emissivity of a surface, three measurements are needed: the voltage from the heat flux sensor and the temperatures of the substrate and the shell. The heat flux sensor output is multiplied by a calibration constant and temperature correction factor to give the heat flux in W/m^2. The heat flux is then used in Equation (2) with the substrate

and shell temperatures to calculate the emissivity of the coating. Figure 4 shows a flow chart of the data reduction process.

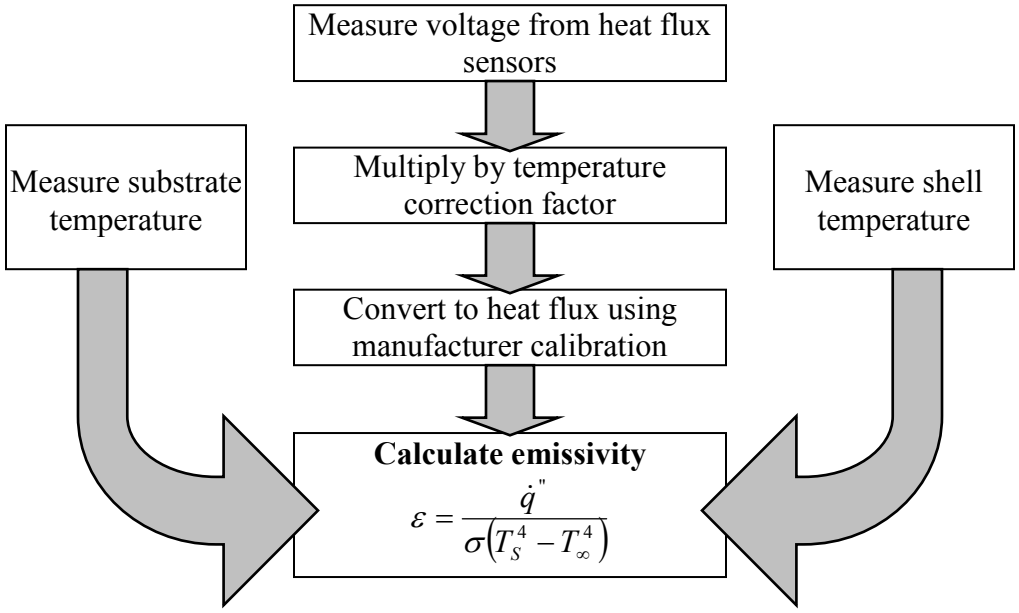

Figure 4. Flow chart showing method of calculating emissivity.

Chapter 4: Ground-Based Experimental Setup

A vacuum chamber was designed and fabricated to test the heat flux-based emissivity measurement technique in the laboratory. The vacuum chamber was designed to hold high vacuum with a pressure lower than 10^{-5} Torr (10^{-8} bar) to eliminate heat loss through conduction and convection. The vacuum chamber consisted of a 25.4 cm (10 in) diameter cylindrical basin, 22.9 cm (9 in) deep with 0.32 cm (0.125 in) thick walls and bottom, capped with a 2.54 cm (1 in) thick by 30.5 cm (12 in) diameter stainless steel flange. The inside of the vacuum chamber was painted black and the chamber was immersed in liquid nitrogen (-195 °C) to simulate radiation to a blackbody or deep space.

A 0.64 cm (0.25 in) diameter Teflon rod 5 cm (2 in) long was used to suspend a high conductivity substrate (copper or aluminum) from the inside of the chamber lid. The heat flux sensors were attached to the side of the substrate facing downward. Since different methods were tested for applying the heat flux sensors, this is discussed in a later section, but the final method chosen was a 0.002 in thick (50.8 μm) film epoxy, Ablefilm 5025E, made by Emerson & Cuming. The coatings to be tested were applied to the heat flux sensor surface by various techniques based on their nature. In the case of paints, the coatings were brushed onto the sensors in two coats. For aluminum and gold tapes, they were applied by hand with latex gloves and pressed down smoothly. A carbon-fiber coating, Vel-Black, was applied using Ablefilm 5025E. Finally, the active coatings tested, the Sensortex ESRs, had heat flux sensors built into the structure. Heaters were attached by pressure sensitive adhesive to the back (top) side of the block to control the substrate temperature. A heat shield made of Mylar multi-layer insulation (MLI) was attached over the heaters to minimize losses from the heaters by radiation.

Several substrates were used depending on the test performed. Initial tests on the small 27160 RdF heat flux sensors used a 3 in x 3 in x 0.25 in copper substrate. The first ESR was tested on an aluminum substrate of the same dimensions. A few tests were done on the large RdF sensors using a 3 in x 6 in x 0.25 in copper block that could hold two sensors of this size. Tests on the module for space used the iridited aluminum housing described later in the section on the Space-Based Experiment. Still other tests used a large 4 in x 6 in (10 cm x 15 cm) aluminum substrate for two large RdF sensors with two Vatell sensors attached to their own substrate that was fixed to the larger substrate by pressure sensitive adhesive.

The chamber lid had four feedthroughs allowing for connection of thermocouples, heat flux sensors, power wires for the heaters, and wires for the excitation voltage of the active emissivity surfaces. The basin wall temperature was measured using three thermocouples installed at different locations. The chamber was connected by a 1.27 cm (0.5 in) outer diameter tube to the vacuum system, which consisted of a turbo-molecular pump and a roughing pump, together capable of sustaining a pressure of 10^{-8} to 10^{-10} bar inside the chamber. The pressure was measured between the turbopump and the vacuum chamber, and was monitored to ensure that it was lower than 10^{-8} bar (7.5×10^{-6} Torr) during tests. Four 0.95 cm threaded rods screwed into the top flange supported the chamber when suspended inside a liquid nitrogen Dewar flask.

Figure 5 shows the assembly of the chamber lid, feedthroughs, and the copper block. Figure 6a shows the vacuum chamber fully assembled, and Figure 6b shows the vacuum chamber installed inside the Dewar flask. A data acquisition system was used to record all the temperatures and heat flux sensors readings.

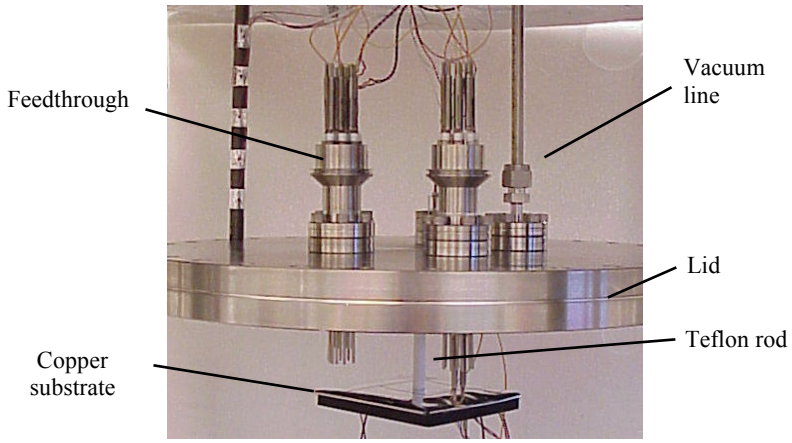

Figure 5. Vacuum chamber lid, feedthroughs, and substrate assembly.

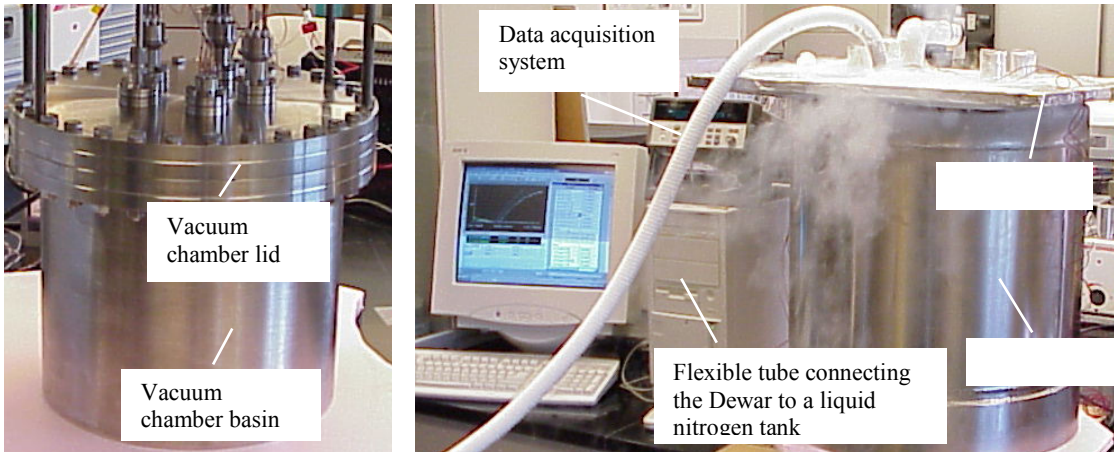

Figure 6. a) Vacuum chamber assembly, and b) the entire experimental setup.

Minimization of Conduction Losses

The conductivity of air is relatively constant with pressure down to the pressure at which the mean free path of the molecules (the average distance between a collision of two particles) is on the same order as a characteristic dimension, such as the distance to the walls of an enclosure.[12, 13] At this point the particles may collide with the walls more often than with each other, thus reducing conduction through the air. The Knudsen number, which is the ratio between the mean free path and the characteristic dimension, is used to calculate the effective change in thermal conductivity at reduced pressures:

$$Kn = \frac{\lambda}{l}$$

An approximate formula for the ratio of effective thermal conductivity of air at reduced pressure and the conductivity at atmospheric pressure is given as: [14]

$$\frac{k_e}{k_0} = \frac{1}{\left(1 + \frac{7.6 \times 10^{-5}}{P * d/T}\right)} \tag{3}$$

where k_e is the thermal conductivity (W/m-K) at reduced pressure, k_0 is the thermal conductivity at atmospheric pressure, P is the pressure in Pa, d is the plate distance in m, and T is the absolute temperature in K. In the vacuum chamber used, the plate distance is about 5.5 in (14 cm).

A pressure of 10^{-8} bar (7.5x 10^{-6} Torr) reduces the effective thermal conductivity of air to 0.8% of its thermal conductivity at atmospheric pressure. With the conduction shape factor for the geometry of this setup ($S = 4\sqrt{\frac{A}{\pi}}$), the result is that conduction through residual air in the chamber represents a heat flux of less than 0.1 W/m^2 at the temperatures experienced, which is small compared to the total heat flux measured (100 to 1000 W/m^2).

Multiple Reflection

In order to prevent the heated surface from seeing its reflection on the bottom of the chamber, a cone was fabricated and attached to the bottom of the chamber as shown in Figure 7. This arrangement increases the likelihood that multiple reflections occur (Figure 7a) before the emitted radiation returns to the copper block. However, since the cone and wall are in reality more like diffuse emitters, it is still possible that some reflection would reach the test surface, as shown in Figure 7b.

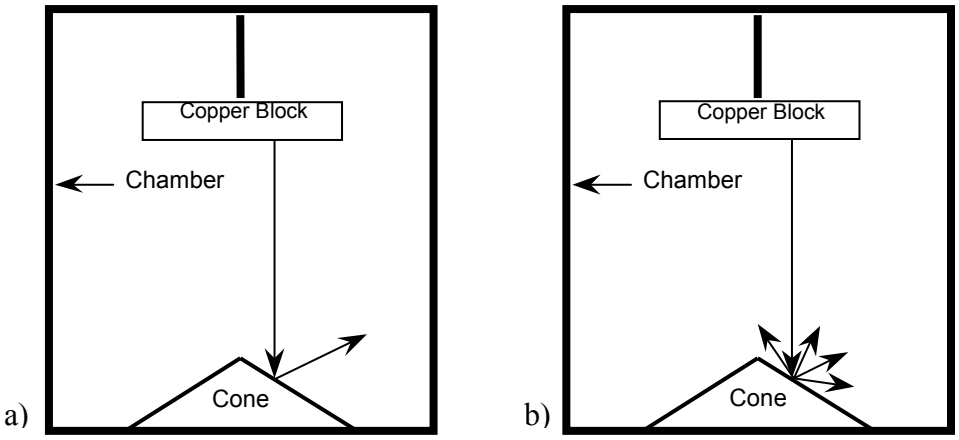

Figure 7. Schematic of the cone position inside the chamber, a) as an idealized non-diffuse surface, and b) as a diffuse surface.

This is accounted for by the fact that the area of the sample surface is much smaller than the inside surface of the chamber, so that the test surface was essentially radiating to a blackbody at liquid nitrogen temperature (-195°C) when the Dewar was filled. The heat flux from the test surface to the enclosure can be written as a two node, source-sink radiation network: [15]

$$\dot{q}_{1-2} = \frac{\sigma T_1^4 - \sigma T_2^4}{\frac{1-\varepsilon_1}{\varepsilon_1 A_1} + \frac{1}{A_1 F_{1-2}} + \frac{1-\varepsilon_2}{\varepsilon_2 A_2}} \tag{3}$$

where surface 1 is the test surface and surface 2 is the inner wall of the vacuum chamber (including the cone). Since the view factor $F_{1-2} = 1$, if $A_2 >> A_1$, the equation becomes:

$$\dot{q}_{1-2} = \frac{\sigma T_1^4 - \sigma T_2^4}{\frac{1-\varepsilon_1}{\varepsilon_1 A_1} + \frac{1}{A_1}} \tag{4}$$

This can be simplified by the following procedure:

$$\dot{q}''_{1-2} A_1 = \frac{\sigma T_1^4 - \sigma T_2^4}{\frac{1-\varepsilon_1}{\varepsilon_1 A_1} + \frac{\varepsilon_1}{\varepsilon_1 A_1}} \tag{5}$$

$$\dot{q}''_{1-2} A_1 = \frac{\sigma T_1^4 - \sigma T_2^4}{\frac{1}{\varepsilon_1 A_1}} \tag{6}$$

$$\dot{q}''_{1-2} A_1 = (\sigma T_1^4 - \sigma T_2^4)\varepsilon_1 A_1 \tag{7}$$

and thus:

$$\frac{\dot{q}''_{1-2}}{\sigma(T_1^4 - T_2^4)} = \varepsilon_1 \tag{8}$$

Equation (8) is the same as Equation (2), showing that the reflected radiation can be safely ignored when $A_2 >> A_1$. In this experimental setup, $A_2 \approx 90 A_1$ for the 2 in x 2 in heat flux sensor; $A_2 \approx 420 A_1$ for the small RdF heat flux sensor.

Data Acquisition and Reduction

The data acquisition system used was an Agilent 34970A data acquisition/switch unit, with an Agilent 34901A 20-channel multiplexer. Temperature and heat flux sensor readings were fed into this system which worked with Agilent BenchLink Data Logger software to display and record the readings on a personal computer screen. The temperatures of several thermocouples on one of the support rods on the outside of the chamber were also monitored on-screen to determine the fill level of the liquid nitrogen. The raw data (temperature and heat flux sensor output voltages) was saved and imported into a Microsoft Excel spreadsheet to perform the heat flux and emissivity calculations and chart the results.

Initial Testing

Testing of the heat flux-based emissivity measurement technique was done both at steady temperatures ("step tests") and while ramping the temperature, either by natural cooling from a preset temperature or using a temperature controller to ramp down and up. As a proof of concept, small RdF (Model 27160) heat flux sensors were attached by pressure sensitive adhesive to a copper substrate, some coated with black spray paint and others with aluminum tape for testing both high and low emissivity coatings. Initial tests showed reasonable results, in which the heat flux readings corresponded well with the theory (see Figure 8), and the emissivity sweep was steady and close to the expected value (see Figure 9). However, in further testing, the heat flux readings sometimes came out so high as to give emissivity values greater than 1. After eliminating conduction and surface roughness as possible causes, pressure effects caused by air bubbles in the adhesive layer were explored as the most likely cause. The next section explains the evidence for this pressure effect and the investigation to find a method of attachment that would give reasonable and consistent results.

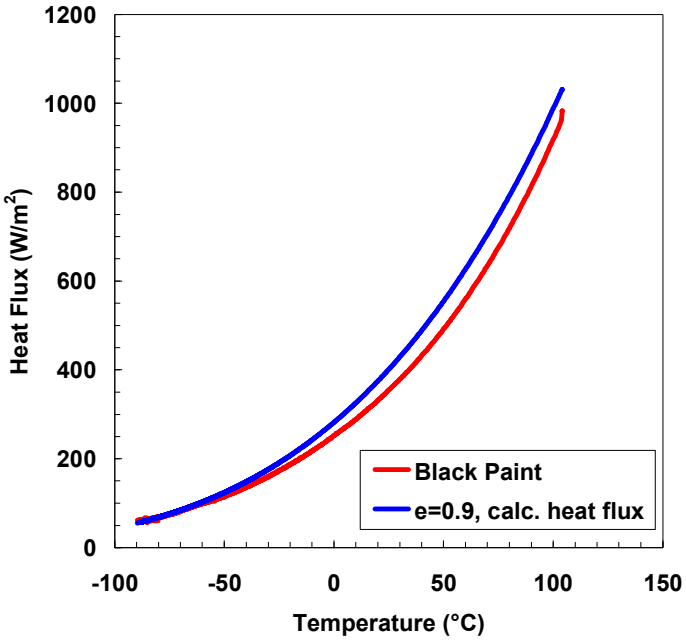

Figure 8. Heat flux reading for black paint, compared to heat flux calculated for an emissivity of 0.9.

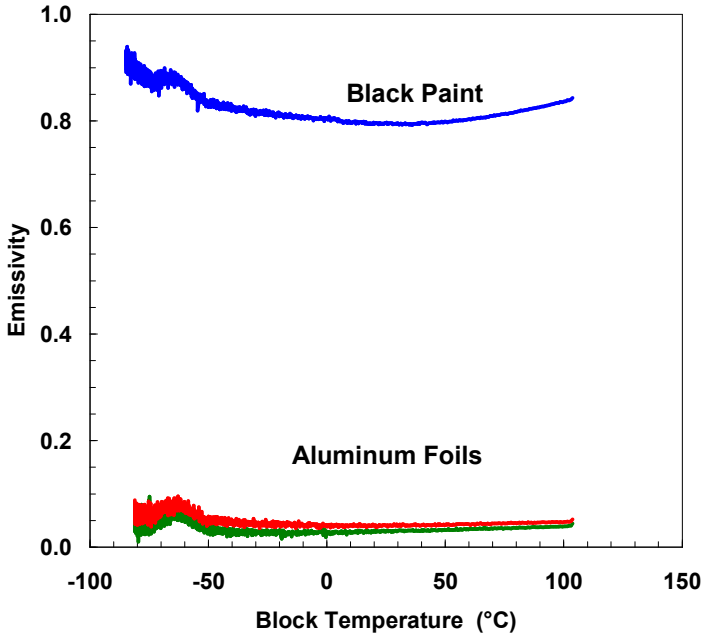

Figure 9. Early measurement of emissivity over a wide range of temperatures. The heat flux sensors were attached to the substrate using PSA.

Method of Attaching Heat Flux Sensors

The first set of tests was performed using the RdF Model 27160 heat flux sensors attached by Minco #10 (3M #966) pressure-sensitive adhesive (PSA) to a 3 in x 3 in x 0.25 in (7.62 cm x 7.62 cm x 0.635 cm) copper substrate. The adhesive was chosen for its ease of application and its low outgassing property. Some of these tests produced reasonable results. Figure 9 shows that the emissivities measured were the nominally expected values. The aluminum coatings were measured with an emissivity of less than 0.1, which corresponds to the highly reflective nature of aluminum and commonly quoted measurements. The emissivity of the black paint was measured as between 0.8 and 0.9, which again fits commonly quoted measurements. Moreover, the emissivities are seen to change only slightly in the range of -100 to 100°C, which is expected for stable coatings. The emissivity of the aluminum coatings is flatter with temperature than the paint, as non-specialized paints may be less stable due to outgassing and material changes with temperature.

However, further testing found that the heat flux readings often drifted upward with time, and the heat flux readings between two sensors experiencing the same heat flux would diverge (Figure 10), as the pressure was decreased to low vacuum. The result was that the heat flux readings were often higher than theoretically possible, giving emissivities greater than 1. The first speculation was that the pressure might not be low enough to eliminate conduction, but the calculation was checked and the pressure was monitored continually, and this was eliminated as a possible cause.

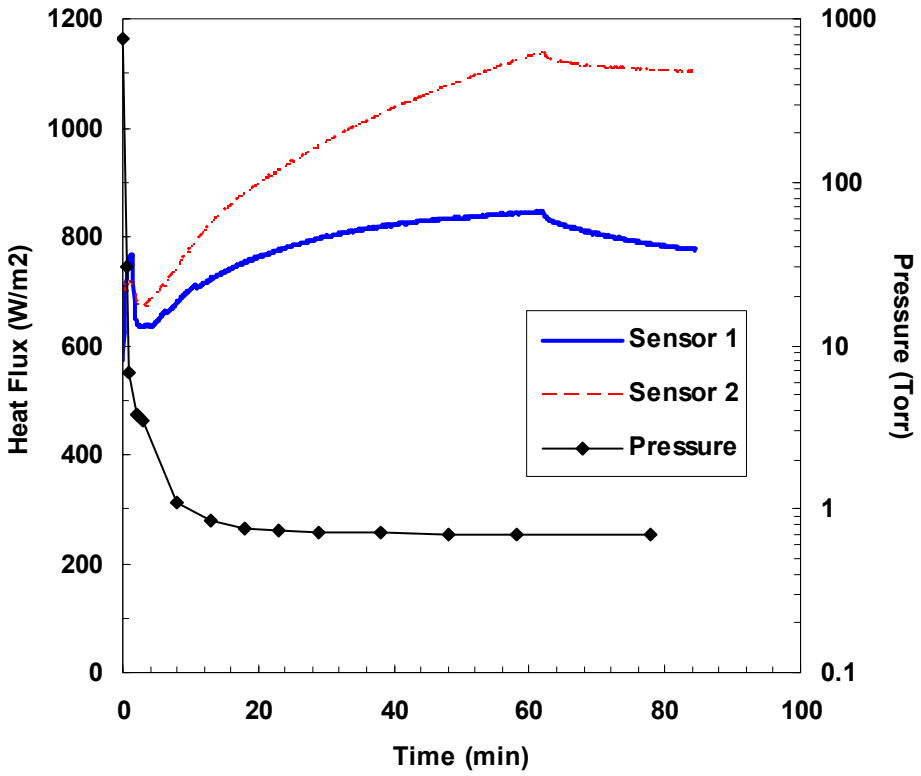

Figure 10. Heat flux readings of two sensors (stacked) as pressure drops to low vacuum.

The high heat flux values and substantial disagreement between sensors were then postulated to be due to expanding air bubbles in the attachment layer, which might cause deflection in the sensor itself. To test this hypothesis, a heat flux sensor was attached to an aluminum substrate with a small hole of diameter about one-third the width of the sensor, covering about 5% of the sensing area. The hole was tapped on the back of the substrate to accept a compressed nitrogen gas line with an NPT connection. The heat flux sensor readings were monitored in atmospheric pressure with heat applied. When the nitrogen supply was turned on to impose pressure on the back of the heat flux sensor, the readings increased substantially (Figure 11). This seemed to affirm the hypothesis. The increase seen here is far greater than that seen in the vacuum chamber tests, probably

because of the large size of the area on which pressure was applied compared to air bubbles in the PSA layer.

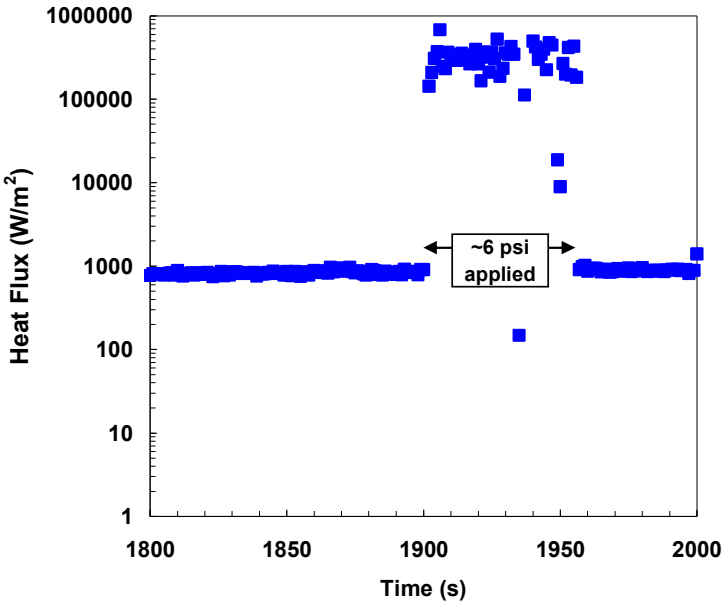

Figure 11. Heat flux sensor reading with pressure applied to the back of a heat flux sensor. The temperature was about 100°C during this test. The semi-log plot is used to show higher resolution on the low values.

The reason for the pressure effect is not understood. RdF states that their heat flux sensors may be used on curved surfaces without affecting their accuracy. Nor should a local bending of the sensor affect the temperature difference across the thermopiles, unless the passive film were significantly squeezed or expanded by the bending or by voids in the layers of the heat flux sensors. In the end, no explanation was established, and it seems that a deeper study into the calibration of heat flux sensors radiating in a vacuum environment would be needed to solve this problem. Indeed, studies of heat flux sensors in various environments have found that calibration results can be highly dependent on the environment.[16]

The attachment method was further refined and greater effort was taken to eliminate contamination and air bubbles in the adhesion layers. Vishay Micro-Measurements gives instructions on surface preparation for the application of strain gages [17] to eliminate contamination, and these were adapted for the attachment of heat flux sensors. The epoxy-phenolic M-Bond 600 sold by Vishay was tested to replace the PSA, but it was found that the curing process caused gas bubbles to form in the adhesion layer. In fact, the mechanism by which M-Bond cures is the release of volatile compounds, which form gas bubbles when there is no way for them to escape. It is designed to be used on strain gauges, which have a much smaller surface area than heat flux sensors.

Eccobond 285 (with Catalyst 24LV) made by Emerson & Cuming was also tested, and produced good results in some runs. Figure 12 shows the results of twelve steady temperature tests on a 2 in x 2 in RdF heat flux sensor attached with Eccobond 285. The emissivity values were fairly steady and close to the expected value (0.935 as measured optically by Sheldahl Corporation, 0.90 as quoted by Lord Corporation), but with a slight shift upward during the progression of tests. However, when the same attachment method was applied to the smaller RdF sensors, the emissivity values were above 1 again and the pressure effect was clearly seen during testing. So again air pockets or voids in the adhesion layer seemed to be an issue (some were visible through the sensor after curing), and these could not be eliminated even when the curing was done in a vacuum bag. It was found that bubbles grew within the uncured, mixed Eccobond upon placing it in a vacuum desiccator at low vacuum. This meant that gases were inherent to the epoxy, and most likely could not be eliminated altogether.

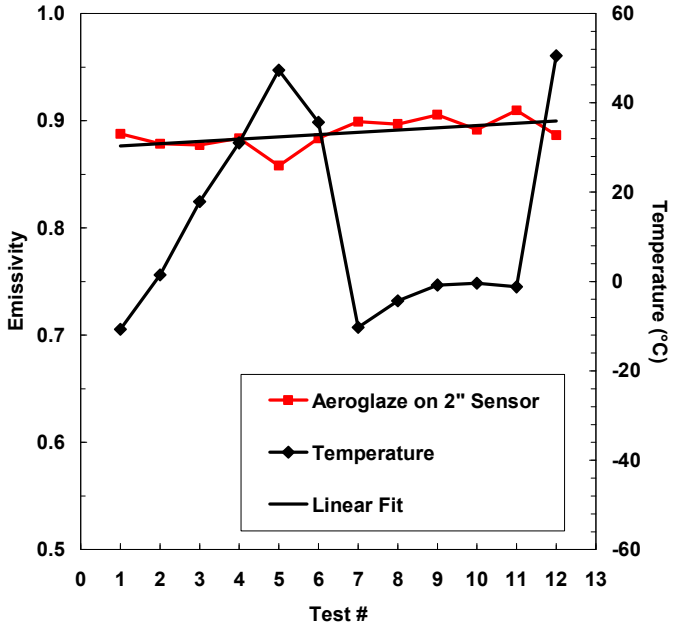

Figure 12. Progression of emissivity tests at various temperatures on Aeroglaze Z306 applied to 2 in RdF sensor which was attached to a substrate by Eccobond 285 epoxy.

The final solution was to use a film epoxy made by Emerson & Cuming, Ablefilm 5025 E, which was used already by Sensortex in the incorporation of the heat flux sensor in their ESR. The cure for Ablefilm is performed at an elevated temperature (150°C for 30 minutes or 120°C for 2 hours) with a vacuum bag, which helps to eliminate air pockets. Ablefilm is also much easier and cleaner to apply than Eccobond or M-Bond, since the film can be cut to size and simply placed on the substrate underneath the heat flux sensor, which no need for brushing or spreading of a liquid. It can also be easily adjusted to the desired position up until the curing process is begun.

The reason for using vacuum bagging in the curing process is both to provide even, constant pressure on the top of the heat flux sensor and to help suck out any air between the sensor and the epoxy layer. Vacuum bagging does not require any special equipment except for a vacuum pump capable of generating a low vacuum. The “bags”

can be made from any flexible, non-porous material (including plastic sandwich bags) with a sealing line of silicone RTV or caulk between the bag and the vacuum tube. In this case, because of the elevated temperatures required for curing the epoxy, a 1-mil (0.001 in) thick, clear polyester film was used that can withstand temperatures up to 300°F (150°C). More detailed instructions on vacuum bagging in general are easy to find on the internet.

Feedthrough Issues

Another difficulty in the laboratory tests was the problem of losing connections at the feedthroughs. During tests, the data acquisition would show bad readings for some sensors and thermocouples inexplicably. Bad readings for the heat flux sensors were recognized usually as output voltages in the range of many millivolts, when the normal level was in the microvolt range. (The 2 in heat flux sensors from RdF would enter the range of 1-4 mV during normal operation, but the small ones would normally remain below 1 mV.) It was not until the last few months of this research, when the connections were taped at the outside of the feedthroughs with aluminum tape, that this problem was identified for certain. The usual way of attaching the wires at the feedthroughs was to thread the wire in at the base of a feedthrough crimp/solder connector and back out through a hole in the side of the connector, then wind the wire around the outside of the connector. While the heat flux sensor wires could be soldered to the connectors (and this was done once), solder was not usually used since a more modifiable setup was desired. However, when aluminum tape was applied to hold the wires and connectors for the heat flux sensors in place, it was noted that the heat flux sensors never again lost their connections as they had in earlier tests. The cause of a lost connection is most likely the

liquid nitrogen. The LN2 may flow into the connector causing the wire to move and lose contact. A photograph of the current method with aluminum tape is shown in Figure 13 below.

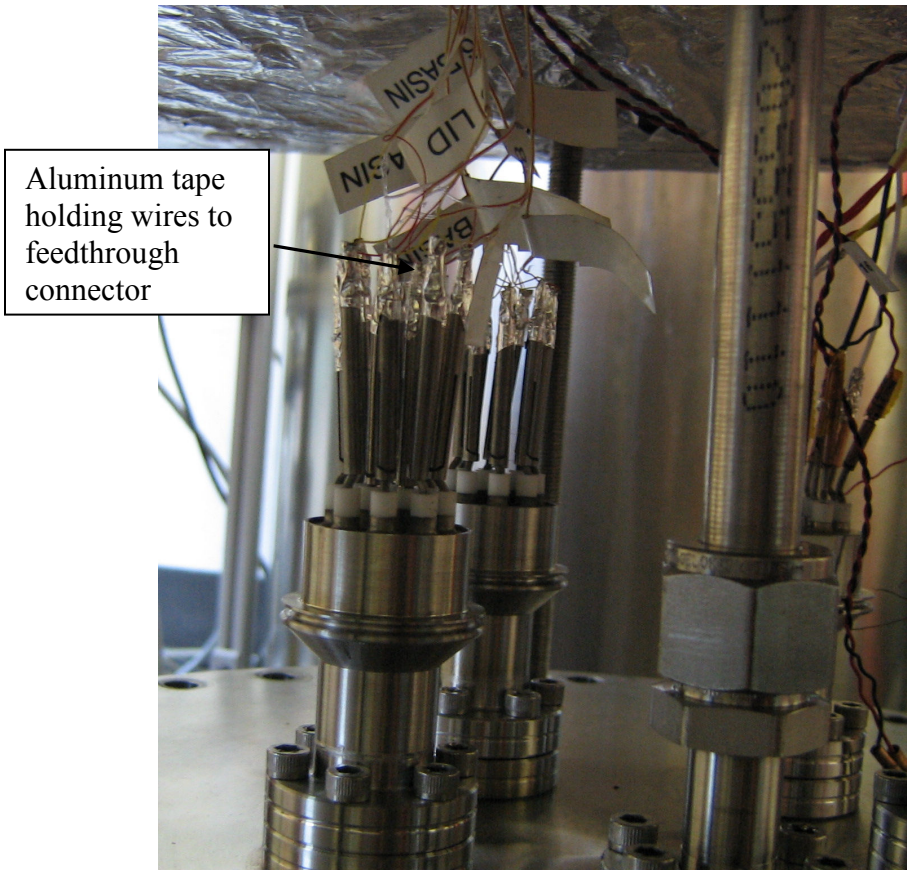

Figure 13. View of feedthroughs on the outside of the vacuum chamber, showing aluminum tape wrapped around wires and connectors.

Chapter 5: Proposed Applications

Passive Surfaces

The advantages of the HFB technique for measurement of passive surfaces were discussed previously and are summarized as follows:

- The heat flux through the sample is measured directly
- Parasitic heat losses do not affect measurements
- The temperature history of sample is not needed
- Lower data volume than calorimetry
- Measurements may be made as temperature varies
- True total hemispherical emissivity is measured
- Multiple surfaces may be tested on one substrate simultaneously
- Samples can be evaluated while operating in space.

With these in mind, the HFB technique is recommended as an additional method of characterizing current and new thermal control coatings, not only where in-space measurements are desired, but in the laboratory as well.

Among the newly-developed passive surfaces is a carbon-fiber appliqué called Vel-Black, made by Energy Science Laboratories, Inc. Its structure consists of thin carbon fibers standing up from an adhesive layer, forming a velvet-like surface with an array of cavities to trap radiation waves. Vel-Black has been measured under conventional techniques as having a solar absorptance of 0.99 and a normal emissivity of 0.95. [7]

The passive coatings used in this research were: Rust-oleum Painter's Touch black spray paint; Aeroglaze Z306 Flat Black paint; Aeroglaze 276A White paint; aluminum tape; gold-coated Kapton tape; and Vel-Black. Table 1 below lists all the passive coatings and their emissivity values, both typical and as tested in a spectrophotometer by Sheldahl Corporation (now called Multek Flexible Circuits, Inc.). The testing and results for these coatings will be discussed later in the section on Laboratory Results of the HFB Technique.

Table 1. Passive coatings used in this research and their relevant properties.

Coating	**Type**	**Color/ Appearance**	**Typical ε**	**ε (Sheldahl)**
Aluminum Tape	Tape	Shiny aluminum	0.1	NA
Gold Tape	Kapton Tape with Gold Coating	Shiny gold	≤0.03	≤0.03 (typical)
Black Spray Paint (Rust-oleum Painter's Touch)	Spray Paint/ Enamel	Flat black	0.85-0.95	0.900
Aeroglaze Z306	Polyurethane Paint	Flat black	0.90	0.935
Aeroglaze A276	Polyurethane Paint	Gloss white	0.90	0.937
Vel-Black	Carbon-fiber appliqué	Black, velvety	0.95	NA

Active Emissivity Coatings

In addition to the advantages that apply to passive surfaces, the heat flux-based technique can measure emissivity changes of mechanically active surfaces which cannot be characterized by optical methods, and can measure sudden changes in emissivity that are difficult to capture by calorimetry. Three active emissivity coatings under development are MEMS louvers, electrochromics, and the Electrostatic Switched Radiator (ESR).

ESRs developed by Sensortex, Inc., were tested in this research to validate the heat flux-based emissivity measurement method.

MEMS Louvers

MEMS louvers are microfabricated versions of the larger scale louvers that were developed earlier for spacecraft. Louvers are vanes that open and close to control the amount of heat radiated from a spacecraft. The outer surface of the louvers have a low emissivity, and the surface beneath the louvers has a high emissivity. Based on the temperature, the louvers are opened to allow the high emissivity surface to radiate, or they are closed to block radiation. They can be controlled without external power using properly calibrated thermal coil springs. Calorimetry test data has indicated changes in effective emissivity of about 0.5 to 0.6 for macro-scale louvers. [8] MEMS louvers work by a similar mechanism, with silicon being the high emissivity substrate, and the louvers being coated with gold for low emissivity. MEMS emissivity control devices have gone through flight validation tests, but are currently showing much smaller emissivity changes. One such device showed an emissivity change of only 0.03. [18]

Electrochromics

Electrochromics are materials whose optical properties are changed by the application of a voltage. Devices for variable emissivity control have been designed using electrochromics that are capable of a considerable change in emissivity/absorptivity with the application of a small voltage.

Variable emissivity electrochromic devices consist of an active element between two electrode layers. The active element consists of three sub-layers: an ion storage layer,

an electrolyte, and the electrochromic. The electrochromic and ion storage layers are metal oxides which exhibit different optical properties in the oxidized and reduced states. When a voltage pulse is applied across the electrodes, ions are moved from the electrochromic layer to the ion storage layer, changing the absorption characteristics of the overall active element. When the voltage is removed, the ions and their associated electrons cannot diffuse back through the electrolyte, and the device remains in the intercalated state. A voltage of opposite polarity is applied to switch back to the unintercalated state. [3, 19]

The top electrode must allow radiation to pass through to the active layer, while the bottom electrode must be reflective. Some electrochromic devices use grids for the top electrode, which can allow about 90% of the radiation through. [3] Eclipse Energy Systems has designed an electrochromic device with a novel transparent, continuous film electrode that exhibits metal-like conductive properties and 95% transmissivity in the measurable infrared region. [19] The continuous film electrode also serves to protect the active element from atomic oxygen in space.

The Eclipse Variable Emissivity Electrochromic Device (EclipseVEECD) uses an activation voltage of about ±1V, and exhibits a high- to low-emissivity ratio of 13.3 at 250 K (absolute emissivities were not given). [19] Another electrochromic device designed at University of Nebraska-Lincoln achieved a low- to high-emissivity range of 0.057 to 0.595, for an overall change of 0.538 and a ratio of 10.4, over the 2 to 13.8 μm range spectral range. [3]

Electrostatic Switched Radiator

The electrostatic switched radiator (ESR) developed by Sensortex, Inc., is a good candidate for validation of heat flux-based emissivity measurements, since it relies on a change in effective emissivity that is undetectable by optical methods. The mechanism is an electrically conductive membrane attached at the four corners so it is suspended in a relaxed state over an electrically conductive plate in a vacuum environment such that a gap exists between the two layers. In this state, heat transfer to the membrane takes place primarily by radiation. When a high voltage (100 to 500 V) is applied, the electrostatic force pulls the membrane down onto the plate, and the heat transfer mode switches to conduction from the plate to the back surface of the membrane. An electrically insulating layer is placed between the plate and the membrane to prevent shorting. The membrane is coated with a low emissivity backing to hinder heat transfer in the inactivated state, yet has a high emissivity surface on the outside so that when activated, it can radiate a considerable amount of heat to space. This allows a large and rapid change in effective emissivity.

To demonstrate this capability, a test module incorporating a heat flux sensor within an ESR was assembled by Sensortex, Inc. A schematic cross-section of the test unit is shown in Figure 14. A custom-made 2 in x 2 in (50.8 mm x 50.8 mm) RdF heat flux sensor was attached to an aluminum substrate using 0.002 in (50.8 μm) thickness Ablefilm 5025E thermally conductive epoxy. A thin (0.032 in, 0.813 mm) aluminum plate was attached to the top of the heat flux sensor such that it covered the sensing area, using the same epoxy film. The aluminum plate was made with a small tab at one corner so a high voltage lead could be attached. It was then coated with an electrically insulating

layer, and the four corners of the ESR membrane were attached to the insulator by PSA such that the membrane was suspended loosely over the insulator when the ESR is not actuated. The membrane material was a thinned Kapton doped with 5% (by weight) carbon, about 15 μm thick. The membrane was also cut with a tab at one corner to connect the other high voltage lead.

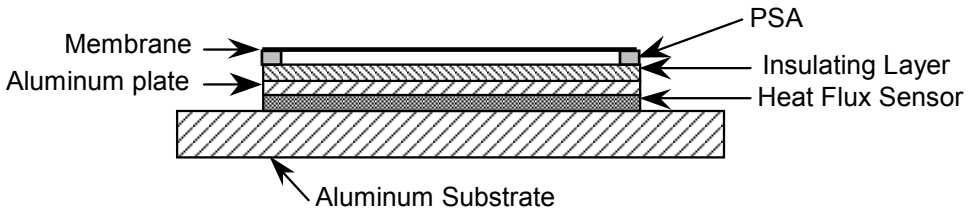

Figure 14. Schematic of an ESR on an aluminum substrate with a heat flux sensor built in (not to scale).

Several models of the ESR/heat flux sensor module were built and tested through the course of this research. Two materials were tested for the insulating layer, Kapton and a barium titanate ($BaTiO_3$)-impregnated polyurethane paint. Also the ESR was tested in two voltage configurations: 1) high voltage on the aluminum plate, membrane grounded; 2) high voltage on the membrane, aluminum plate grounded. The second configuration was chosen for the space experiment. In this configuration, different voltages were tested to determine the emissivity change with respect to voltage applied. The size of the aluminum substrate was also changed between models for incorporation into the MISSE-6 space flight experiment. The results of the ESR tests are also explained in the section on

Laboratory Results of the HFB Technique. A photograph of a $BaTiO_3$ ESR is shown in Figure 15.

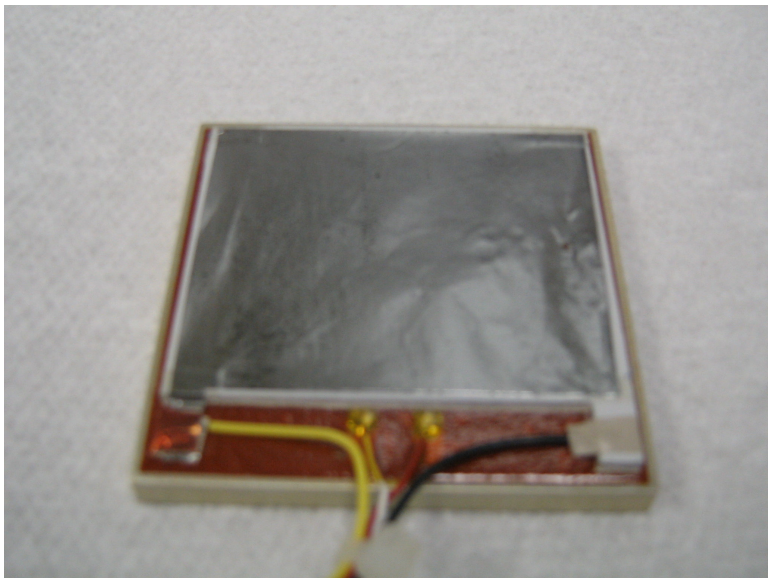

Figure 15. Sensortex ESR with $BaTiO_3$ insulator (white in color), incorporating a heat flux sensor for HFB emissivity measurement.

Chapter 6: Laboratory Results of the HFB Technique

Passives Surfaces

Initial testing was performed on passive coatings to demonstrate the validity of the emissivity measurements taken by the heat flux-based method. Along the way, two important issues were discovered: 1) the importance of attachment method (heat flux sensor to substrate) in the function of the heat flux sensor; and 2) discrepancies in the manufacturer-supplied calibration and temperature correction of the heat flux sensors. Considerable testing was needed to resolve these issues.

Ablefilm 5025E film epoxy, applied using vacuum bagging, was found to be the best attachment technique to avoid air bubbles or voids in the attachment layer. However, even with this attachment the heat flux sensors were found to yield emissivity values greater than 1 at times. Further, the temperature correction given by Vatell seemed inaccurate, especially at temperatures below 0°C, based on both steady temperature and ramp emissivity tests. Vatell quotes a 0.01% change in sensitivity per degree Celsius away from 25°C (increased sensitivity above 25°C). RdF, however, gives the temperature correction for their heat flux sensors in the form of a quadratic curve-fit from -300 to 400°F (-184 to 204°C). RdF also gives a fifth order curve-fit (a more precise version of the quadratic) in the datasheets provided with the custom-made sensors:

$$y = 5E\text{-}14\ x^5 - 2E\text{-}11\ x^4 - 6E\text{-}09\ x^3 + 3E\text{-}06\ x^2 - 0.0016\ x + 1.1$$

where x is the temperature in °F, and y is the multiplication factor for the heat flux sensor output. The base temperature (multiplication factor = 1.0) is 70.0°F (21.1°C).

It was finally decided that for the purposes of the emissivity measurement technique, a known emissivity coating should be tested in the vacuum chamber, adjusting

the manufacturer's calibration value and temperature correction to match the known emissivity. This way, all factors affecting calibration and temperature correction in the high vacuum environment are accounted for. However, if this recalibration is needed for each individual sensor, it would detract from the feasibility of the HFB emissivity measurement method. Thus further research is suggested to determine whether one correction test would apply to all sensors of a certain model. A more scrupulous review of the manufacturer's heat flux sensor calibration method would also be helpful for future work, and may eliminate the need for any adjustments to the calibration factors.

Recalibration & Temperature Correction Tests

A series of steady temperature ("step") tests were performed on two of the custom-made 2 in x 2 in RdF sensors, and two 1 in x 1 in Vatell sensors, all coated with Aeroglaze Z306, to determine new calibrations and temperature corrections for the sensors. The two RdF sensors were epoxied to a 4 in x 6 in x 0.25 in (10 cm x 15 cm x 0.64 cm) aluminum substrate, and the two Vatell sensors were epoxied to their own smaller 1.1 in x 2.2 in 0.188 in (2.8 cm x 5.6 cm x 0.478 cm) iridited aluminum substrate (as used in the space-based experiments described later), which was attached to the main substrate by PSA. Thermocouples were placed on both the main aluminum substrate and the smaller Vatell substrate.

Tests were performed on this set of sensors over about 10 weeks' time, and the results were analyzed as they were performed. Based on the step tests, corrected sensitivities and temperature corrections were calculated that would give a temperature-independent emissivity close to 0.935 as measured optically by Sheldahl. This was done three times, using a new set of step tests to perform the calculation each time. One

temperature correction was calculated for the two RdF sensors and another for the two Vatell sensors, in both cases using 21.11°C (70°F) as the base temperature as RdF did. However, one of the Vatell sensors appeared to deviate more than the other in later tests, so an individual temperature correction was calculated for it the third time. A quadratic equation was found to be sufficient for the temperature corrections, so the 5th order equation provided by RdF was abandoned. The temperature correction for all the sensors turned out to be close to the one supplied by RdF; the 0.01% correction supplied by Vatell was much too low at the extreme temperatures. The last set of step tests with the temperature correction applied are charted in Figure 16, which shows all of the emissivity values within 2% of the optically measured value.

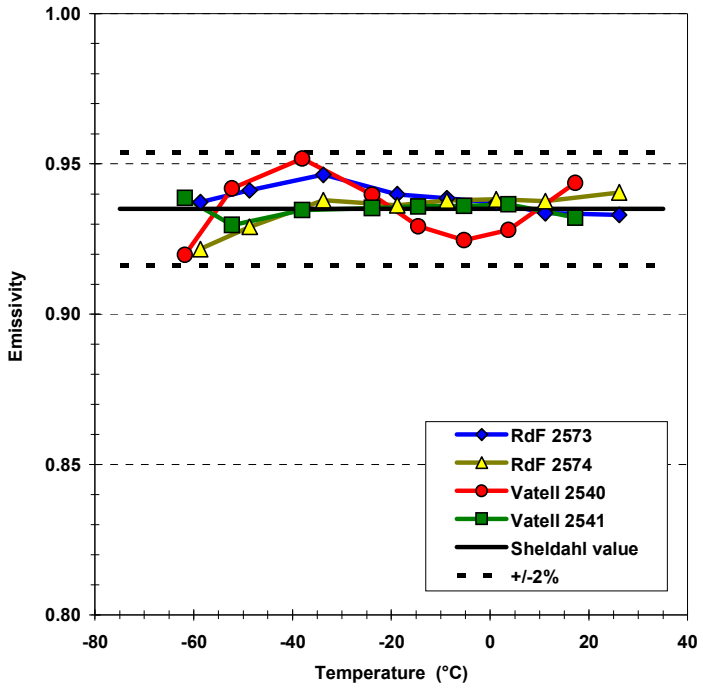

Figure 16. Step tests from which the temperature correction was calculated, with the correction applied.

Once the calibrations and temperature corrections were calculated, they were applied to ramp tests as shown in the following charts, Figure 17 through Figure 20.

While one of the Vatell sensors (#2540) behaved differently, the ramp test for three of the four sensors indicates that the heat flux transience did not affect the results very much when the proper temperature correction was used. In other words, tests do not need to be performed at steady temperatures to get accurate results, as was hypothesized in the original design of the system. The same results are charted by emissivity versus temperature in Figure 21 and Figure 22. The one issue that still remains is that there seemed to be a slight shift in the readings from the earlier tests to the later ones. That is, the calibration calculated for the first several tests didn't work as well when applied to later tests. Further discussion of the recalibrations and is given later in the section on Error Analysis for Emissivity Measurements. Results of laboratory tests on other passive coatings are shown in the section on Laboratory Testing of the MISSE Module.

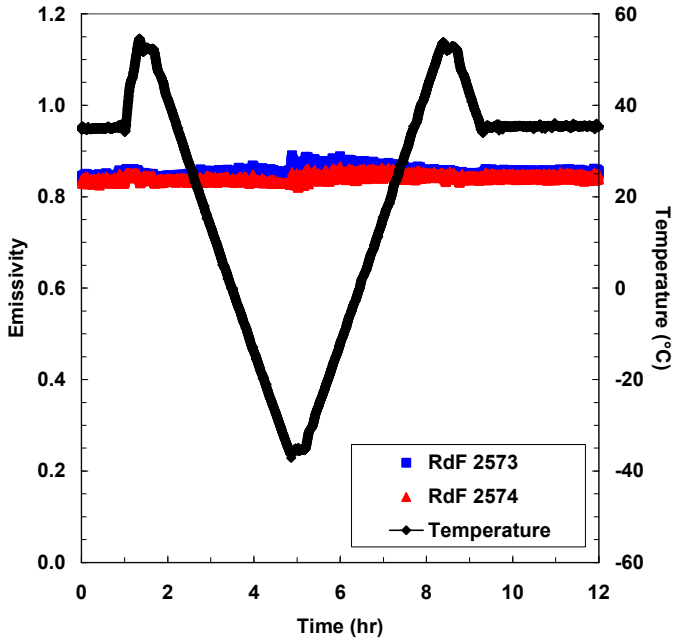

Figure 17. Ramp test of Aeroglaze Z306 on RdF sensors using the original manufacturer's calibration sensitivity and temperature correction (smoothed by 7-point moving average).

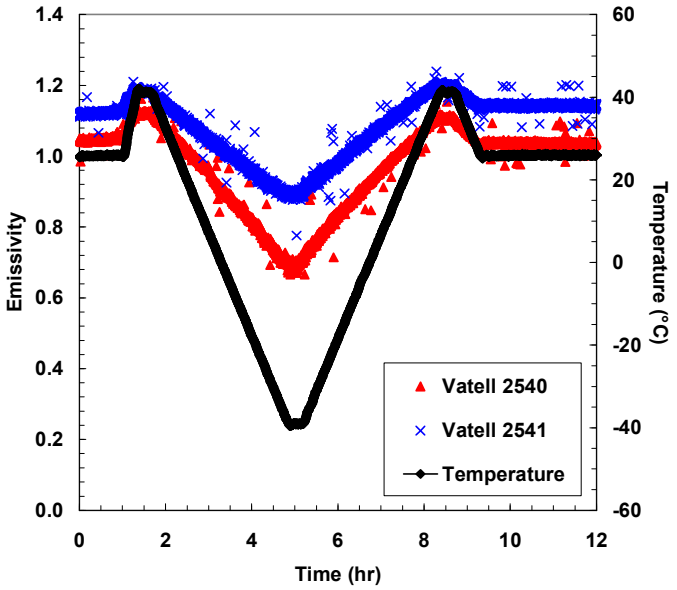

Figure 18. Ramp test of Aeroglaze Z306 on Vatell sensors using the original manufacturer's calibration sensitivity and temperature correction.

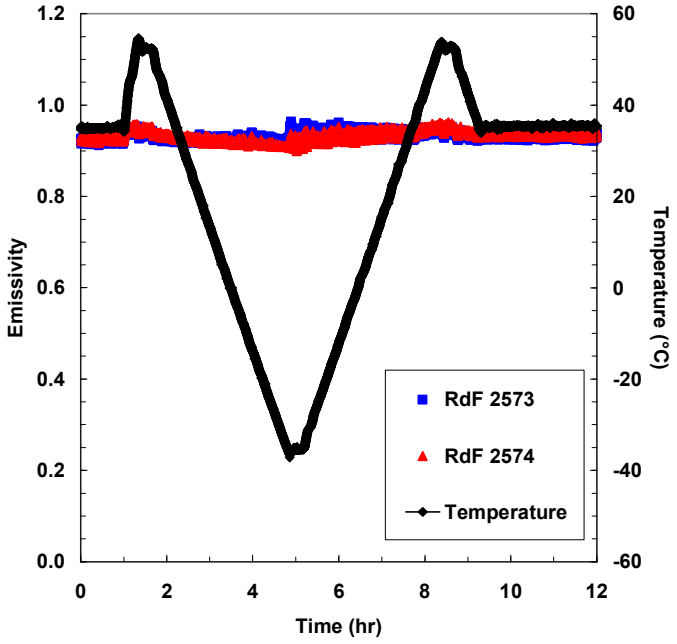

Figure 19. Ramp test of Aeroglaze Z306 on RdF sensors after applying new sensitivity and temperature correction factors.

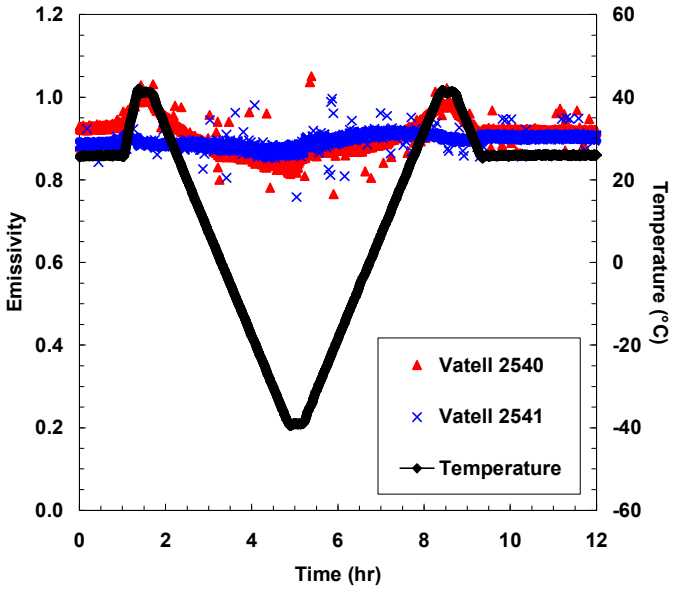

Figure 20. Ramp test of Aeroglaze Z306 on Vatell sensors after applying new sensitivity and temperature correction factors.

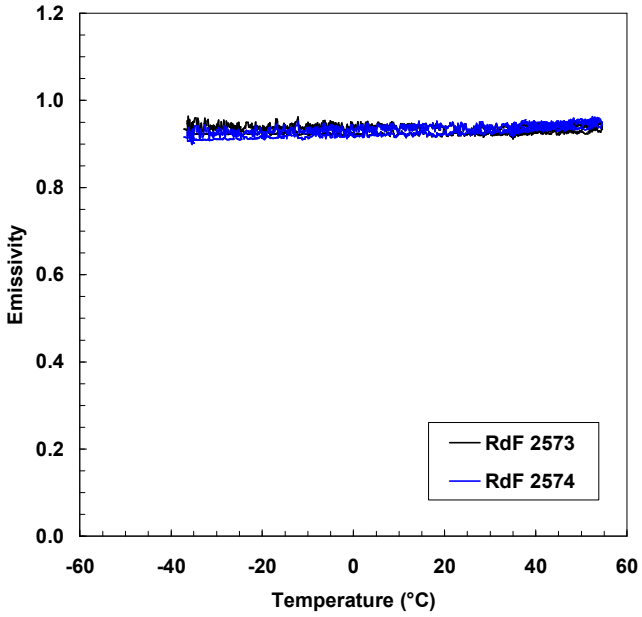

Figure 21. Emissivity versus temperature from ramp test of Aeroglaze Z306 on RdF sensors with new sensitivity and temperature correction factors. (Same test as Figure 19.)

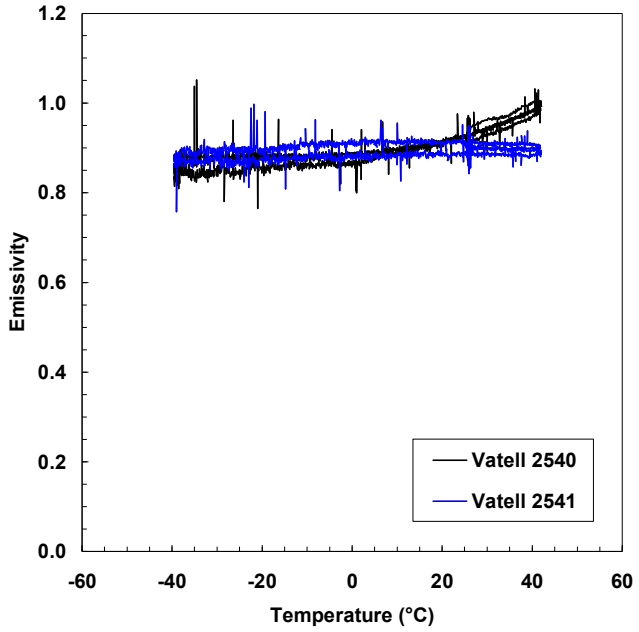

Figure 22. Emissivity versus temperature from ramp test of Aeroglaze Z306 on Vatell sensors with new sensitivity and temperature correction factors. (Same test as Figure 20.)

Active Surfaces

The active surfaces tested in this research were a number of ESRs developed by Sensortex, Inc. Several different versions of the ESR were tested, as there were continual developments based on the testing. The most significant issue seen in testing the ESRs was that the membranes did not always fully detach (seen in the measurements as the emissivity not immediately returning to the original ground-state value). Therefore the design was altered to improve this.

Initial ESR Tests

The first ESR was tested in the vacuum chamber by itself on an aluminum substrate similar to the copper substrate used for the early passive tests. High voltage lines were

connected to the feedthroughs, but otherwise the setup was essentially the same as for testing the passive coatings.

Figure 23 shows results obtained from the first ESR tested, activated at 315 V. When actuated, a stark peak was seen in the heat flux sensor reading, corresponding to an apparent emissivity of much greater than 1. This transient behavior is due to sensible heating of the membrane by conduction, which when deactivated is receiving very little heat from the body of the ESR. When activated, the membrane comes into good thermal contact with the structure of the ESR beneath it and it takes time for it to reach the temperature of the rest of the ESR. In the first tests, this transient portion was seen to disappear within about 10-15 seconds, though the settling time varied somewhat among test runs. The effective emissivity settled to a value more than 0.6 higher than the original ground state. This $\Delta\varepsilon$ is on the same order as the louvers currently employed on satellites, a very good confirmation of the ESR's potential for thermal control.

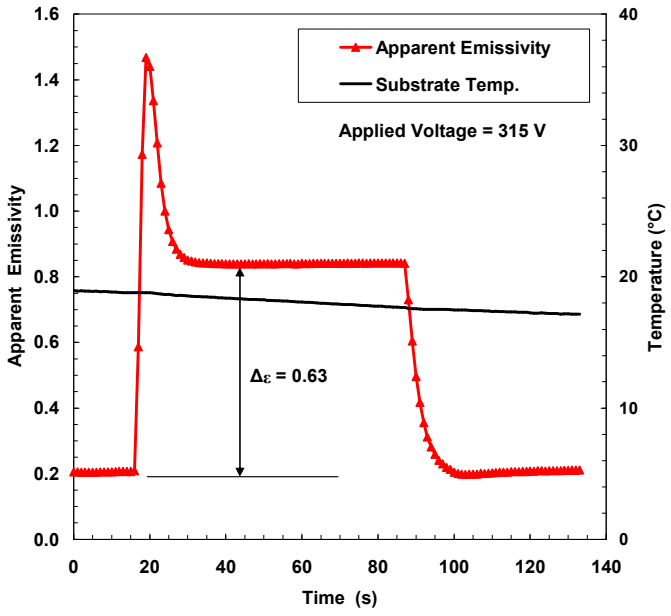

Figure 23. Results for the first ESR tested in the vacuum chamber.

ESR Performance with Variation of Actuation Voltage

The ESRs were tested at various voltages to see how this would affect the effective emissivity of the activated state. The results for two ESRs at 40°C are shown in Figure 24 and Figure 25. As expected, higher voltages gave a higher Δε than lower voltages since the electrostatic force on the membrane is greater. In earlier ESR models there was a big change in the behavior from 200 V to 300 V, but this pair showed the highest dependency on voltage below 200 V. The ideal is to use the lowest voltage possible while getting an adequate Δε, because of the cost of high voltage amplifiers and because of safety concerns where high voltages are present. Sensortex has been continually assessing their membrane material and the insulating layer used, since these are the major factors affecting the extent of contact when the ESR is activated.

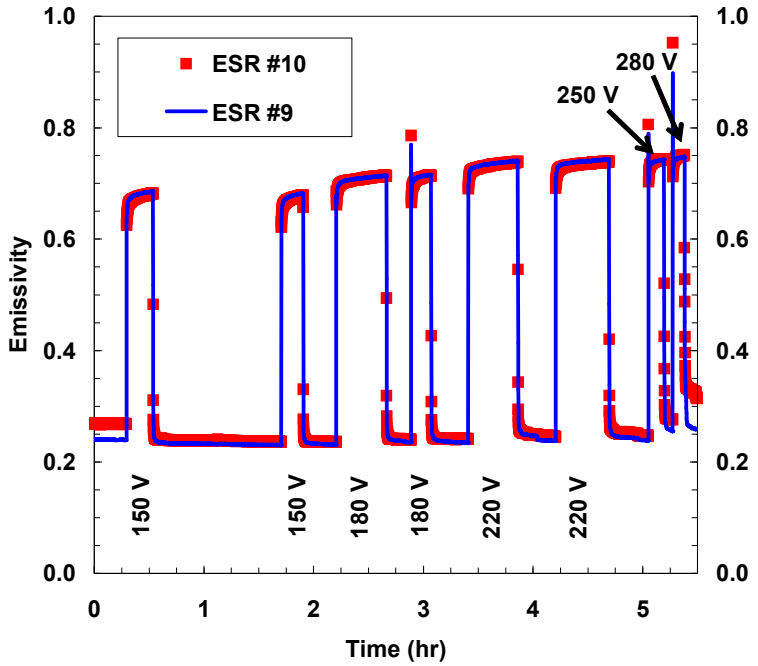

Figure 24. Activation of two ESRs at various voltages, tested using the HFB method.

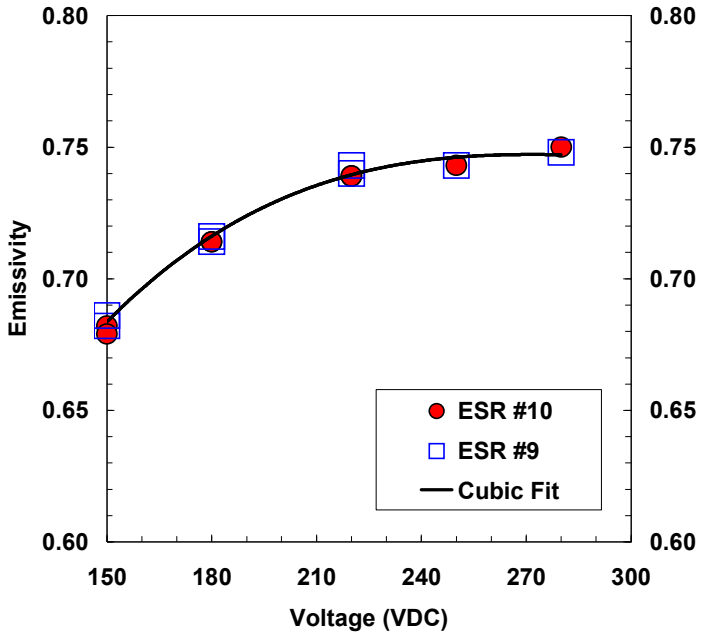

Figure 25. Activation of the ESRs showing the emissivity versus applied voltage (same data as previous figure).

Membrane Sticking

One difficulty that was seen in testing the ESRs was that when deactivated, the membrane would not always fully detach. In the vacuum chamber test data, this was seen as the effective emissivity not returning to its original deactivated value when the voltage was removed. It was also visible to the eye when the ESRs were activated outside the vacuum chamber. Membrane sticking tended to occur after activating the ESRs for many cycles and for long periods of time. This is a problem in the operation of the ESRs, which needed to be dealt with for their own validation as well as for the space-based tests, since if the membrane continued to stick more and more in subsequent cycles, and would not return to a low emissivity, there might not be any useful results after a few cycles. Figure 26 shows an example of a test performed on two ESRs, showing significant sticking as

the ESR cycles. The problem seemed to worsen with longer actuation time and the number of cycles that the ESR had already undergone.

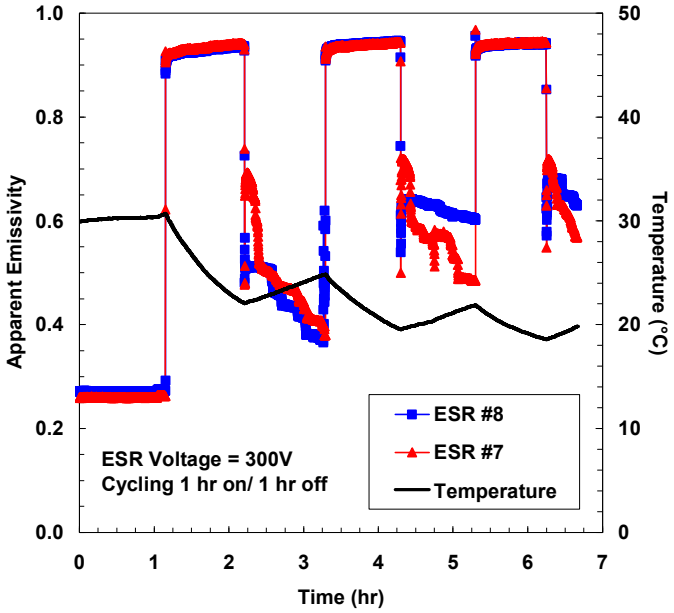

Figure 26. Test results on ESRs #7 and #8, showing that membranes did not fully detach after each cycle.

As shown in Figure 27, the membranes detached after several minutes in this test. The time needed to detach also seemed to lengthen with the length of actuation. This was problematic if the ESRs were to be actuated for 12 hours at a time as planned for the MISSE experiment. The cause of the sticking was not immediately understood, and it was not clear whether it was a "mechanical" sticking such as everyday sticky substances exhibit, or an electrical sticking in the sense that the electrostatic force had not fully dissipated.

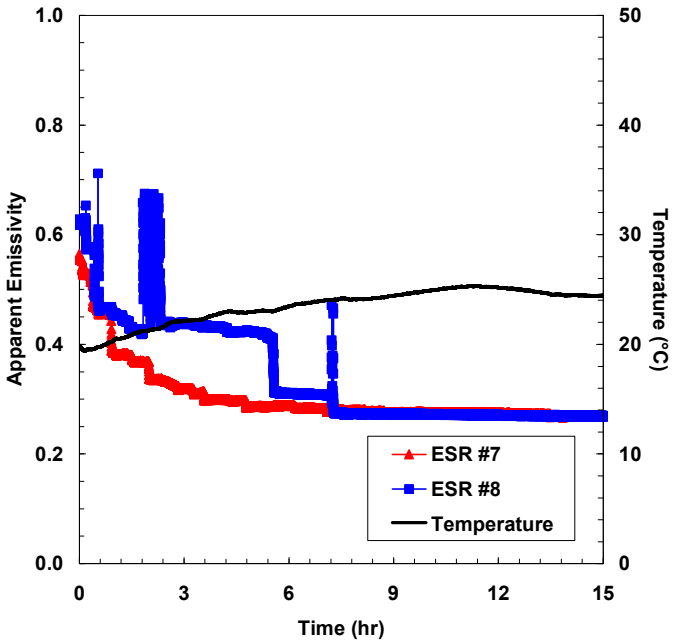

Figure 27. ESRs detach after several hours and return to original ground state.

To test whether the problem was one of residual charge, a reverse polarity on the ESR was tested. At first the leads were simply reversed to change the polarity, but when this seemed to have no effect a power supply with the capability of providing a high negative (with respect to ground) voltage was tested. At the end of one test when the ESRs exhibited sticking, the high negative voltage (-280 V) was applied for a period of 1 minute and then the voltage was completely turned off. After this the ESRs quickly dropped to the expected deactivated range, as shown in Figure 28. Moreover, the subsequent tests showed no sticking, suggesting that discharging the ESR in this way had a lasting effect on the ESR's ability to discharge the voltage upon deactivation. It was decided to incorporate the negative polarity voltage into the MISSE module, and to have it turn on for 1 minute following every 12 hour "on" portion of the ESR cycle. This way, it is hoped that the ESRs will always be fully discharged before they are activated each time.

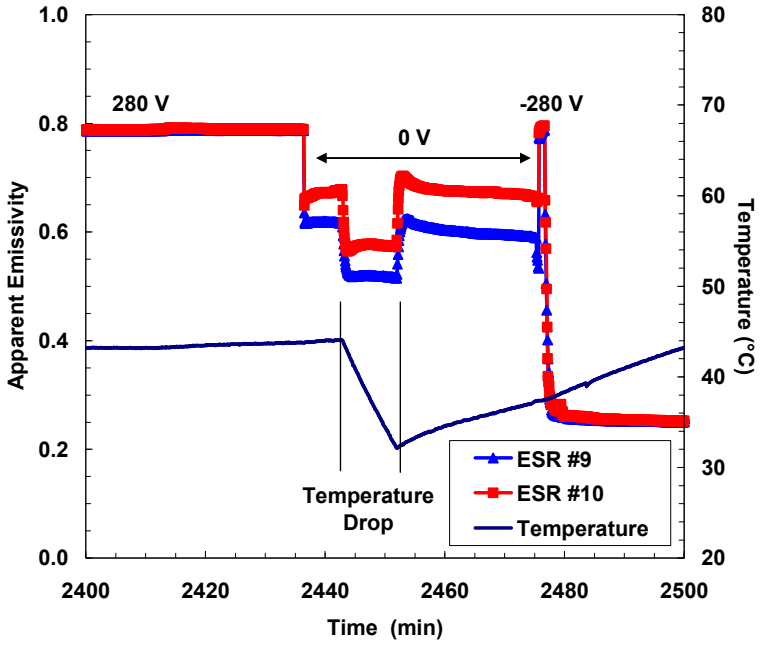

Figure 28. Test showing sticking of ESRs and de-sticking when a high negative voltage was applied for one minute.

The issue of sticking was further explored by testing two different insulating materials, since the insulator was thought to be the most likely part holding charge. The coating of the membrane which allows it to be polarized is conductive (aluminum). While in an open circuit (as when the two leads are simply disconnected from the ESR) it might not immediately lose its charge, in some tests the leads were disconnected and put together so that the membrane and aluminum plate were at equal potential, and the membrane still did not immediately detach. The design being used at this time employed a barium titanate ($BaTiO_3$)-impregnated polyurethane paint (Imron 3.4 HG-C, impregnated with $BaTiO_3$ to 36% by volume) as the insulating layer, while Kapton had been used in some previous ESR designs. So a new ESR was built with a Kapton insulating layer, and this was tested in the vacuum chamber along with the $BaTiO_3$ ESR. A test that illustrates the different performance of the two is graphed in Figure 29, which

shows that the ESR with the Kapton insulator reached a higher effective emissivity in the activated state. However, these two ESRs were not seen to stick in any subsequent tests, even without the negative voltage applied, before the MISSE module was sent to JHU-IDG to have the electronics installed, and after that only tests of the fully integrated module including the negative voltage were performed, so no sticking data was obtained for the ESR with the Kapton insulator. The results of these tests are shown in the chapter on the space-based experiment. The reason why the Kapton ESR reached a higher emissivity is not clear. The two possibilities that immediately came to mind were 1) that the Kapton has a higher thermal conductivity and therefore provides less thermal resistance; and 2) the Kapton may have a lower surface roughness, giving less contact resistance. However, the first may not be explanatory because of the added adhesive layer required for attaching the Kapton. The second was found to be untrue when the surface roughness of two samples were measured using a profilometer.

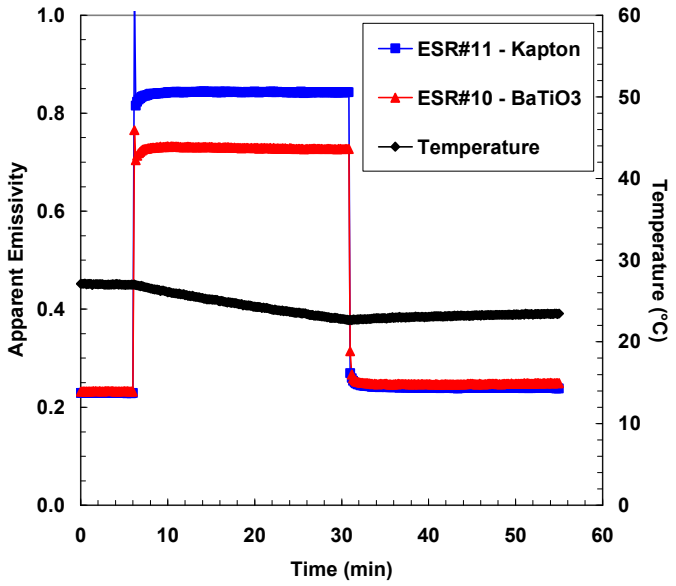

Figure 29. Comparison of ESR with barium titanate ($BaTiO_3$) insulator and with Kapton insulator actuated at 200 V.

Numerical Modeling of ESR Behavior

A numerical model of the ESR was developed for comparison with the experimental data. In order to capture the transient behavior during activation, the ESR model was set up with the membrane attached to the skin, but the membrane was given an initial temperature lower than the skin temperature. This way, the simulation could predict the heat transfer starting from the instant the ESR is actuated, including the sensible heating of the membrane.

The initial temperature of the membrane was calculated using the radiation network for a thin film of uniform temperature receiving radiation from a source (ESR assembly) and emitting to a sink (chamber walls) as shown in Figure 30.

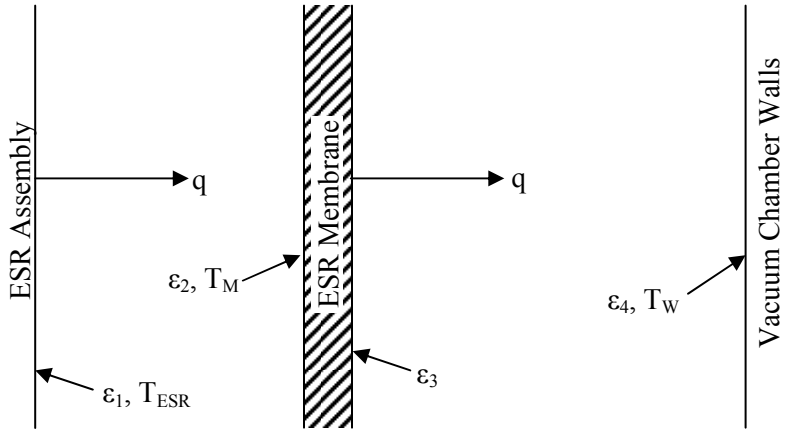

Figure 30. Schematic for calculating the temperature of the ESR membrane in deactivated state.

This network can be solved using two equations. The heat flux from the ESR assembly all the way to the chamber walls is given by

$$\dot{q} = \frac{\sigma\left(T_{ESR}^4 - T_W^4\right)}{\frac{1-\varepsilon_1}{\varepsilon_1 A_1} + \frac{1}{A_1 F_{1-2}} + \frac{1-\varepsilon_2}{\varepsilon_2 A_2} + \frac{1-\varepsilon_3}{\varepsilon_3 A_3} + \frac{1}{A_3 F_{3-4}} + \frac{1-\varepsilon_4}{\varepsilon_4 A_4}} \tag{9}$$

while the heat flux from the ESR assembly to the membrane only is given by

$$\dot{q} = \frac{\sigma\left(T_{ESR}^4 - T_M^4\right)}{\frac{1-\varepsilon_1}{\varepsilon_1 A_1} + \frac{1}{A_1 F_{1-2}} + \frac{1-\varepsilon_2}{\varepsilon_2 A_2}} \tag{10}$$

where the emissivities and temperatures are defined as in Figure 30. The subscript 1 is used for the ESR assembly, subscripts 2 and 3 for the respective sides of the membrane, and subscript 4 for the vacuum chamber walls. The view factors F_{1-2} and F_{3-4} are both 1, assuming that the surface of the ESR only sees the membrane, and the outer surface of the membrane only sees the chamber.

Since the heat flux to the membrane is the same as the heat flux to the chamber walls, the two can be solved simultaneously to find the temperature of the membrane.

Given a temperature of 25°C (298 K) for the ESR and -195°C (78 K) for the chamber walls, the temperature of the membrane is calculated to be about -100°C (173 K). The emissivity used for the external surface of the membrane was 0.882, the value measured optically by Sheldahl Corporation, and the emissivity used for the aluminum-coated side was 0.1. The emissivities of the other surfaces were estimated from known values of similar materials.

However, the calculated initial temperature of the membrane is significantly affected if ε_2 (low emissivity side of the membrane) is changed. Since the values estimated for aluminum-coated Kapton range from 0.017 to 0.202 [10], this could cause an error in the simulation's peak value. A lower value will give a higher temperature difference (meaning the initial temperature is less than -100°C), giving a higher peak value of heat flux, and the opposite is true for higher emissivity values. Another factor that affects the initial temperature of the membrane is the attachment points. The corners of the membrane were attached to the plate by small areas of PSA. Conduction can take place in this region, causing the initial temperature of the membrane to be closer to that of the main assembly. For this reason the initial temperature was also varied in some of the simulation runs, to obtain a peak heat flux value closer to that of the experimental results.

Results of the Numerical Model

The ESR was modeled as a discrete ordinates radiation problem in Icepak software, which uses the Fluent solver. As stated before, the membrane was modeled in contact with the insulating layer without the PSA. Screenshots of the model are shown in Figure 31 through Figure 33, where the mesh is displayed on the heat flux sensor surface. The

inside surface of the vacuum chamber was modeled as a cylinder closed at both ends at -195°C (78K), with a surface material of high emissivity black paint. The vacuum was approximated as air at atmospheric pressure with the appropriate reduced thermal conductivity, since Icepak is not optimized for solving radiation in a vacuum by specifying pressure. The material properties (specific heat capacity, thermal conductivity, and density) of some layers in the ESR had to be approximated due to lack of available data, such as the epoxy (Emerson & Cuming Ablefilm 5025E) and the polyurethane paint that acts as the electrical insulator. The heat flux through the heat flux sensor was the value of interest extracted from the numerical simulations.

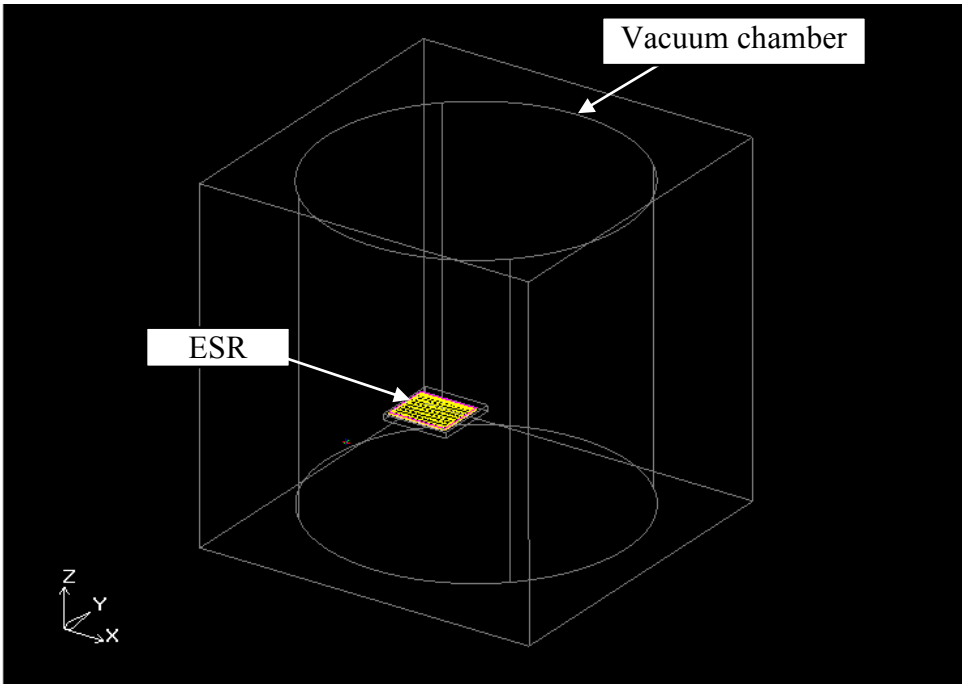

Figure 31. Screenshot of ESR model.

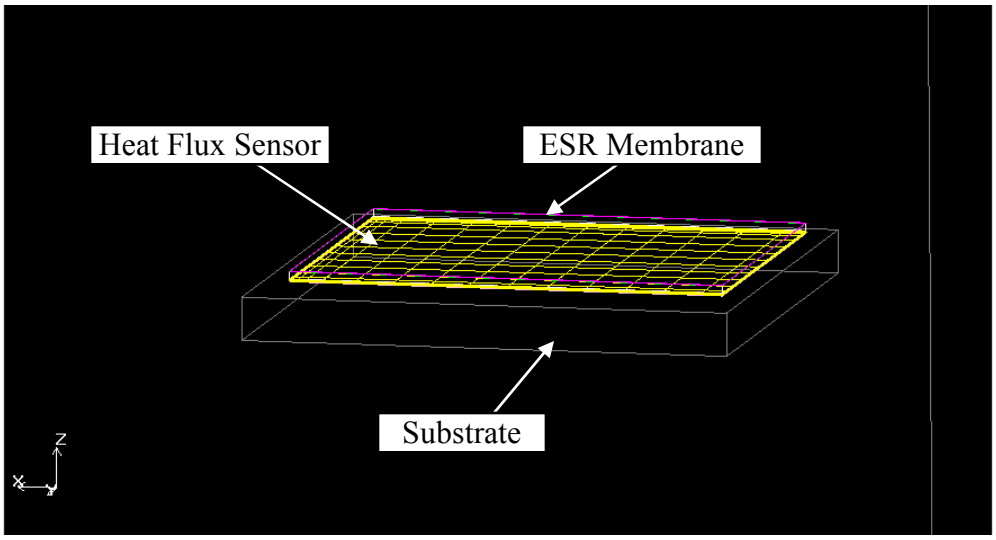

Figure 32. Close-up of ESR in model. Heat flux sensor mesh is shown.

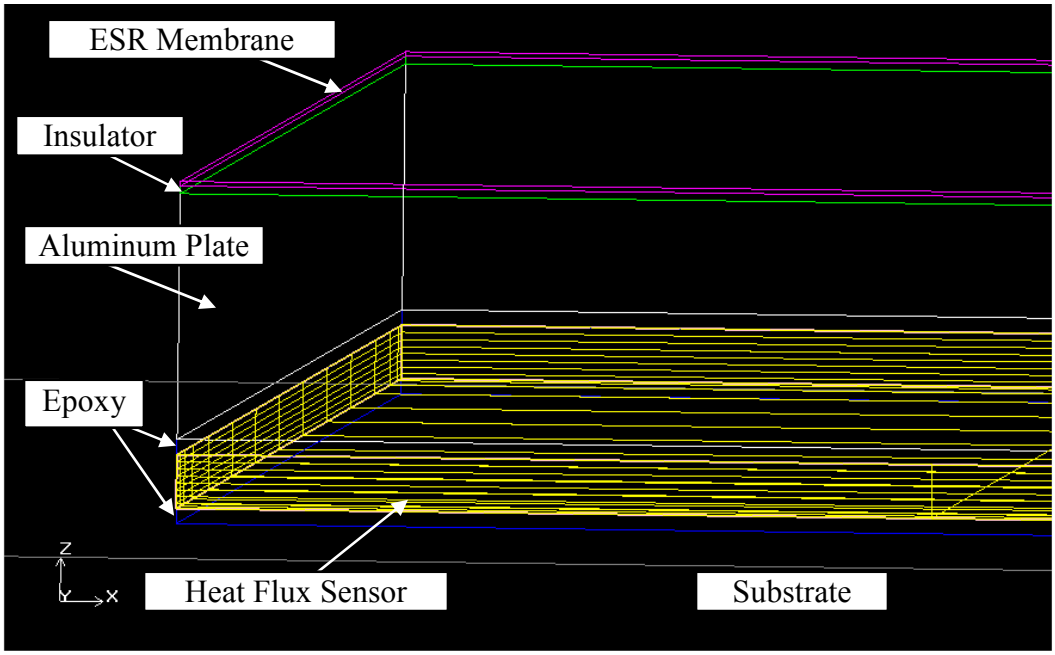

Figure 33. Close-up of ESR layers in model. Mesh is shown on the surfaces of the heat flux sensor.

The simulation was run with a varying time step: 0.1-second steps for the first 2 seconds, 0.2-s steps from 2 to 4 seconds, 0.5-s steps from 4 to 8 seconds, and 1-s steps from 8 to 10 seconds, with an end time of 10 seconds. The simulation results (Figure 34) showed a heat flux variation qualitatively similar to the experimental results, from the instant of ESR activation to the heat flux value in the steady activated state. The heat flux reaches a steady value of about 400 W/m^2, which is on the same order as the

experimental results. The time constant is also on the right order. The maximum heat flux value in the spike is about 1800 W/m^2, much higher than what is seen during experiments. This may be due to an inaccurate (too low) calculation of the membrane's initial temperature caused by using approximate emissivities or due to conduction through the PSA that attaches the membrane at the corners.

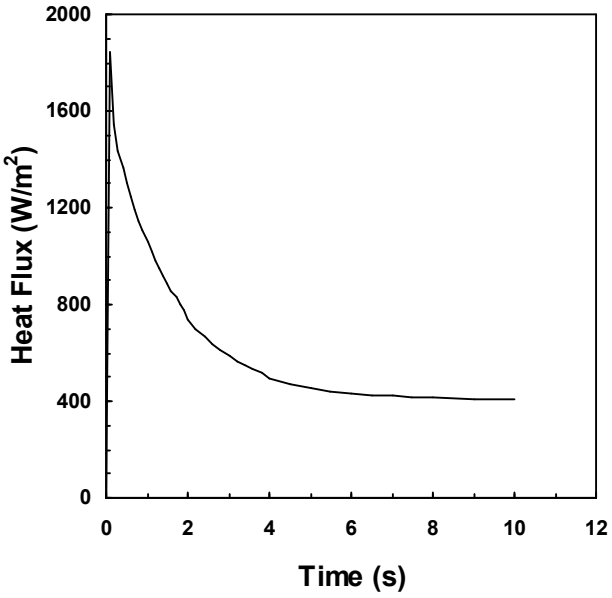

Figure 34. Heat flux through the ESR predicted by numerical model.

Verification of Numerical Model

The time steps and the mesh parameters were varied one at a time to determine if there was any change in the solution. Table 2 and Figure 35 show the setup for the three variations in time steps. The time steps were decreased first for just the first 4 seconds,

Table 2. Step sizes (in seconds) for the transient runs.

	0-2 s	**2-4 s**	**4-8 s**	**8-10 s**
1st Run	0.1	0.2	0.5	1
2nd Run	0.05	0.1	0.5	1
3rd Run	0.05	0.1	0.2	0.5

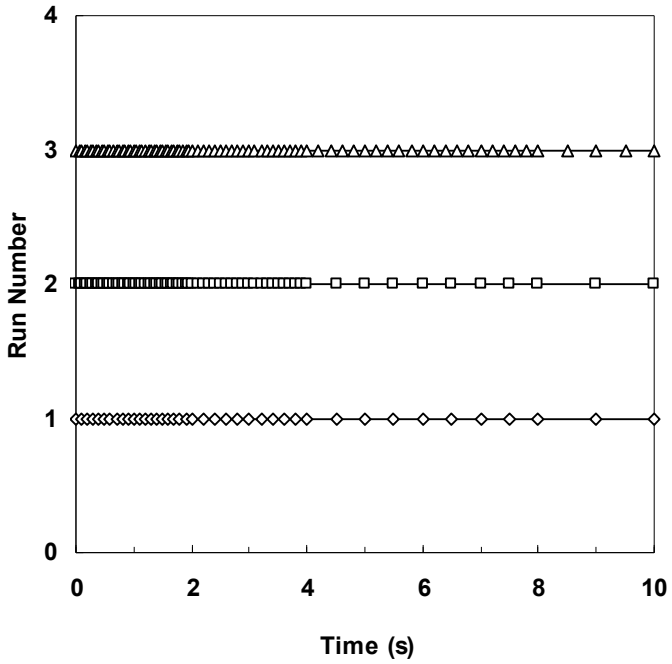

Figure 35. Variations in time step for ESR transient simulation.

and approximately the same solution was obtained. The only difference was that a higher peak value was found in the run with the finer time step, about 2400 W/m^2 as opposed to 1800 W/m^2 which is expected since the heat flux at time t = 0 is infinite. The time steps were then decreased for all 10 seconds, and still the same solution was found, again with the higher peak value. The results of the three runs are shown together in Figure 36.

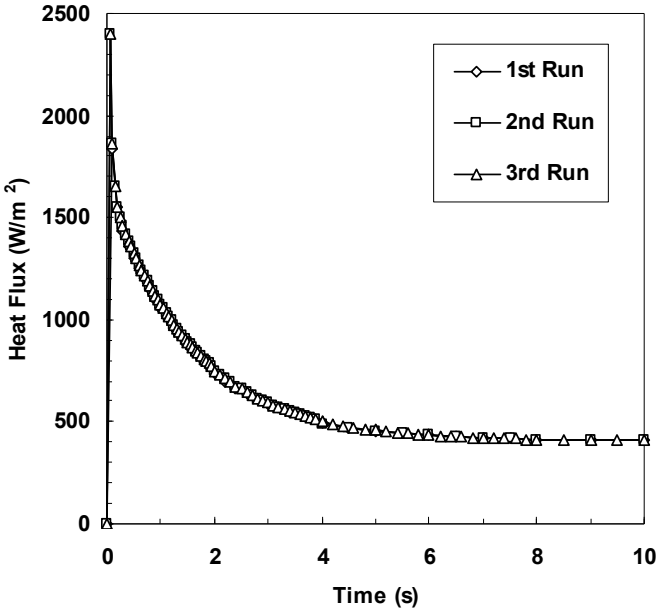

Figure 36. Comparison of solutions with different time step settings.

The mesh density was also varied while using the original time steps. The number of elements in the layers were increased in two steps to determine if they affected the solution. As an example, the heat flux sensor was originally given a count of 7 elements in the direction normal to its face, and the membrane was given a count of 3 in the same direction. Figure 37 shows a close-up view of this mesh in the heat flux sensor. These were increased to 10 and 5, respectively, for the next run, and further increased to 12 and 7 in a subsequent run. Figure 38 shows the results of the three runs together. The solution exhibited no dependence on the mesh density.

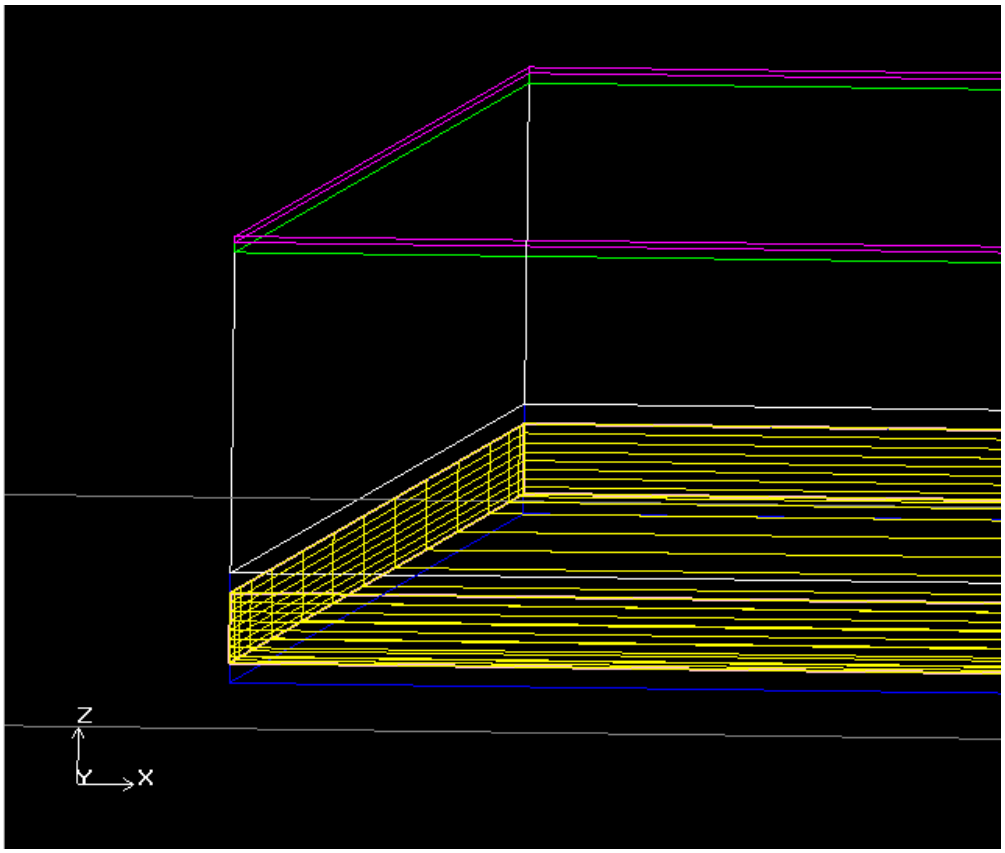

Figure 37. Initial mesh in heat flux sensor layer.

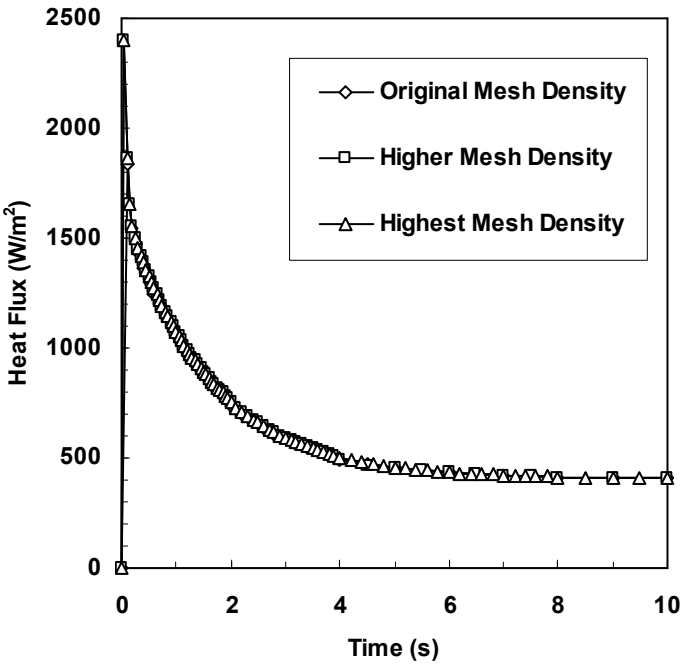

Figure 38. Comparison of solutions with different mesh densities.

Variation of Initial Membrane Temperature

As stated above, the initial membrane temperature calculated is highly dependent on the estimated emissivity of the aluminum coated underside of the ESR membrane. Sources give different values for the emissivity of aluminized Kapton, taken from different measurement methods. The values given by Jaworske and Skowronski [10] range from 0.017 to 0.202 as measured by two optical instruments and a calorimeter. Further errors may be present due to wrinkles and other imperfections in the membrane caused by the repeated activation and relaxation. The simulation was run with the membrane at several different initial temperatures to see what effect this had on the solution. A chart comparing these simulations is shown in Figure 39. Also plotted on this figure are experimental results from two ESRs, one with an insulating layer of $BaTiO_3$, the other with Kapton. Note that the experimental results were taken with the substrate at 14°C, while the simulations were run with a substrate temperature of 25°C. The actuation voltage in the experiments was 280 V. The simulations show higher spikes than the experimental results, as the simulations do not consider heat "leaking" into the membrane from the ESR structure, when in reality there is some heat transfer by conduction through the PSA at the corners of the membrane. Thus it makes sense that the simulations with higher initial temperatures (closer to the temperature of the main ESR assembly) drop more quickly towards the values seen in the actual operation of an ESR. Also note that while the simulations had an initial temperature of 25°C for the main assembly, the two ESRs shown in the chart were at about 13°C in this case.

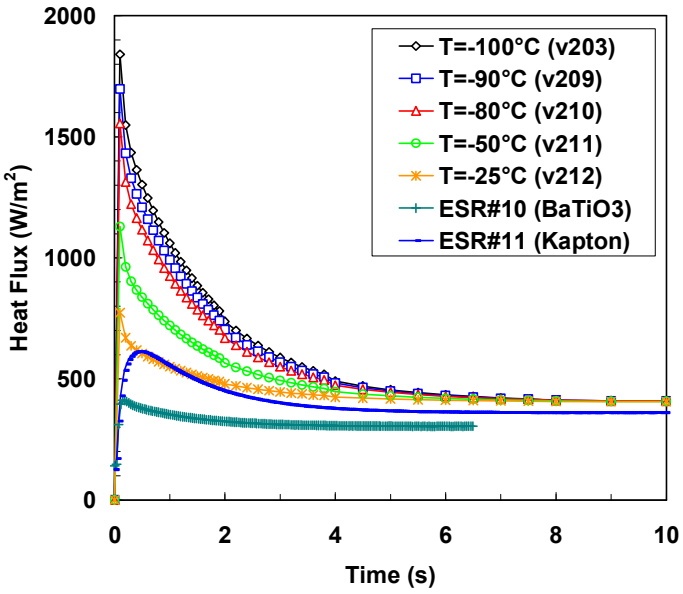

Figure 39. Comparison of simulations using different initial temperatures for the membrane, plotted with experimental results for two ESRs.

Chapter 7: Error Analysis for Emissivity Measurements

Potential sources of error in the HFB emissivity measurements include the blackbody assumption (no radiation reflected back to the test surface), radiation from the edges of the sensors and coatings, temperature difference between the surface and the substrate, measurement errors, and errors in the recalibration of the heat flux sensors.

As stated in the section on Multiple Reflection, if the area of the sink surface is much greater than the area of the emitting surface, reflected radiation is negligible and the blackbody assumption is valid. In the case of the large sensors, the area of the chamber walls was about 90 times the area of the sensor/coating, and in the case of the small sensors the ratio was about 427. When the emissivity calculation was performed for a sample set of data, the emissivity calculated was different by 0.001 for the large sensors, and 0.0002 for the small sensors, which turns out to be small compared to measurement errors. When the HFB technique is used in space, the error due to the blackbody assumption should approach zero when the module is radiating out to deep space, depending on how much (if any) of the ISS is in the way of its view.

A second possible source of error is the effect of radiation from the edges of the sensors and coatings. However, the geometry of the heat flux sensors is such that radiation from the edge of a sensor does not substantially affect the readings. The RdF heat flux sensors are 0.007 in (0.178 mm) thick, and the thermopile junctions closest to the edge are 0.025 in (0.635 mm) from the edge. This distance is large enough that heat flowing through the sensing area will not radiate out the edge of the sensor and will only radiate out the edge of a test surface if the sample is very thick. (The temperature of the outer surface of the sensor, including the edges, may be considered uniform, since all of

this surface is in radiative transfer with the chamber walls.) In the case of the ESR and the Vel-Black casing, the thickness is dominated by a low emissivity surface: the aluminum plate in the case of the ESRs, iridited copper for the Vel-Black. This prevents the edges from radiating an appreciable amount of heat. Moreover, the area of the heat flux sensor edges is less than 4% of the top surface area for the small RdF sensor, and even lower for the large sensors. Thus radiation from the edges of the sensors and coatings can also be considered negligible. If the HFB method were applied to a thick coating with high emissivity edges, the heat flux measurement should be multiplied by the ratio of the total test surface area (including edges) to the top surface of the heat flux sensor.

Another potential error is the difference between the substrate temperature and the actual surface temperature. This error becomes important when the surfaces applied to the heat flux sensors are thick and have a low thermal conductivity. Given the low heat flux in these tests, this does not apply for the coatings being tested in this study. Even for the ESRs, which are relatively thick, the temperature drop is dominated by the heat flux sensor and not the layers of the coating. The temperature drop was calculated to be about 0.74°C across the RdF heat flux sensors for 500 W/m^2 heat flux, which is typical for the high emissivity coatings in the vacuum chamber. The error associated with a 1°C temperature offset is only about 1.6 %. It should be kept in mind, however, that the location of temperature measurement may be important. As explained later in the section on Laboratory Testing of the MISSE Module, a significant difference was seen between the temperature inside the flight housing (where the electronics were located) and the outside surface of the housing where the samples were mounted. If desired,

thermocouples may even be placed on the sample or heat flux sensor (some heat flux sensors may be purchased with built-in thermocouples).

Measurement Errors

Recalibration of the sensors aside, the measurement error can be calculated using the heat flux sensor calibration error combined with all other measurement errors. The measurement of emissivity depends on the measurement of heat flux, surface temperature, and the temperature of the vacuum chamber walls. Therefore, the thermocouple and heat flux sensor calibration errors as well as measurement errors in the data acquisition unit contribute to uncertainty in calculated emissivity. A root-mean-square analysis was used to combine these uncertainties as

$$\Delta\varepsilon = \sqrt{\left(\frac{\partial\varepsilon}{\partial\dot{q}''}\Delta\dot{q}''\right)^2 + \left(\frac{\partial\varepsilon}{\partial T_S}\Delta T_S\right)^2 + \left(\frac{\partial\varepsilon}{\partial T_\infty}\Delta T_\infty\right)^2} \tag{11}$$

The thermocouples used were type *K* with an uncertainty of ±2.2°C for subzero and ±1.1°C for above-zero temperatures, and the data acquisition contributes another 1°C error in temperature measurement. RdF claims their heat flux sensors are calibrated with 3-5% error, with infinite resolution over the entire heat flow range.[20] Vatell does not state their calibration error. The data acquisition contributes only 0.0050% error in voltage readings. Because the heat flux sensor measurements also depend on the temperature correction factor, the error in the surface temperature measurement was combined with the heat flux sensor output error (calibration error and data acquisition error) to provide a root-mean-square error for the heat flux. The heat flux error $\Delta\dot{q}''$ is given in terms of the output error ΔV and the surface temperature error ΔT_S as

$$\Delta\dot{q}'' = \sqrt{\left(\frac{\partial\dot{q}''}{\partial V}\Delta V\right)^2 + \left(\frac{\partial\dot{q}''}{\partial T_S}\Delta T_S\right)^2} \tag{12}$$

Because of the dependence on temperature error, the error is lower if the temperature used in the calculation is an average of several thermocouples on the substrate. If four thermocouples are used, as was done in some tests, the temperature error turns out to be half the error of an individual thermocouple. When only two thermocouples are used, as in the MISSE module, the temperature error equals the error of an individual thermocouple divided by $\sqrt{2}$. This means the error in the temperature measurement with two thermocouples is ΔT_S =±1.1°C for temperatures above zero and ±1.7°C for temperatures below zero.

Combining the temperature errors for the surface and the chamber walls with the sensor calibration error, the heat flux error for a small RdF sensor in the range of 60°C to -60°C is calculated as 5.0% to 6.7%. The emissivity error is calculated to be between 5.2% and 7.4%, or ±0.05 to ±0.07 in the emissivity value. Because of the low heat flux and the temperature measurement error, the emissivity error is largest at the lowest temperatures.

The heat flux error for a high emissivity passive coating test on a large RdF sensor turns out to be about 5.2% to 5.4% over the range of 40°C to -40°C. This translates to an emissivity error of about 5.5% to 5.9%, or ±0.05 to ±0.06 in the emissivity value, where again the highest emissivity error is at the lowest temperatures.

For testing an ESR at room temperature on a large RdF sensor, the heat flux error was calculated to be about 5.8%. The corresponding emissivity error is about 6.0%, or about ±0.04 in the activated state and ±0.01 in the non-activated state.

Recalibration Errors

A precise calculation of the error in recalibrating the sensitivity value and temperature correction factor for the heat flux sensors would require a standardized calibration process with many sensors. However, the error for the set of sensors recalibrated in this study may be estimated by comparing all the ramp test data with the latest corrections applied, to the expected emissivity value of the coating. This error was calculated for each data point as the difference between the emissivity value obtained and the expected value (0.935) divided by the expected value,

$$Error = \frac{\varepsilon_{measured} - 0.935}{0.935}$$

Most of the ten ramp tests were done from 40°C to -40°C and back up, though the last three included temperatures as high as 60°C and as low as -60°C. A 7-point moving average was applied to the emissivity values for the RdF sensors, to smooth out constant fluctuations. After calculating the error for each data point, the average and standard deviation of the errors were calculated for each heat flux sensor in each test. Figure 40 shows the average errors, and Figure 41 shows the standard deviations.

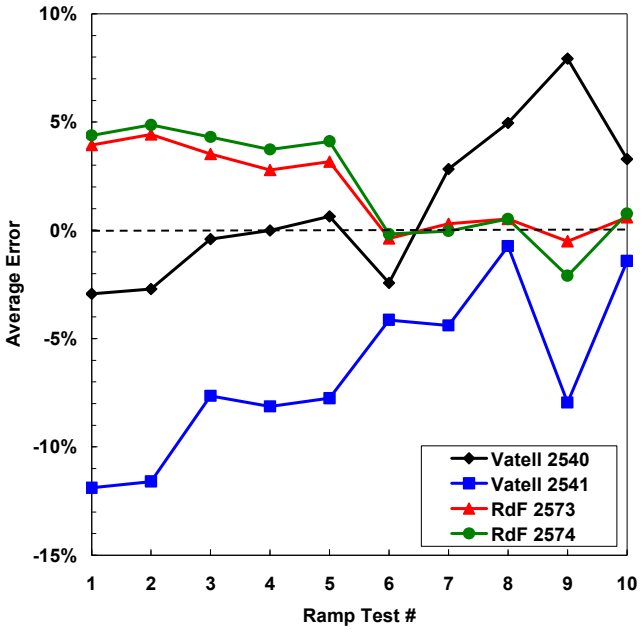

Figure 40. Average errors for each heat flux sensor when calculated corrections were applied.

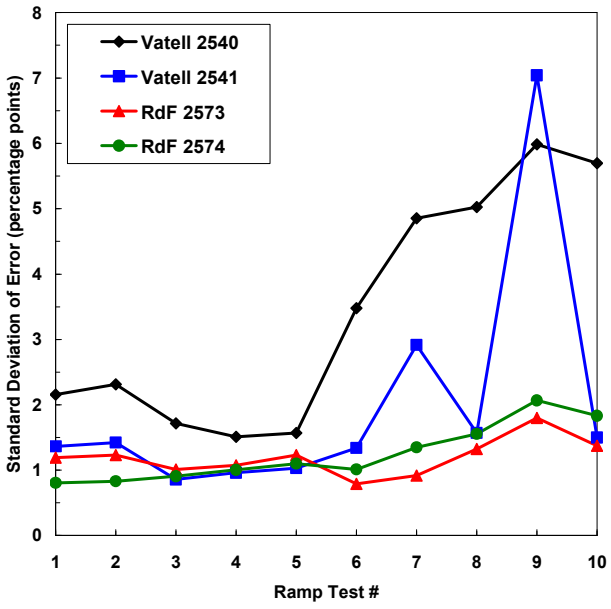

Figure 41. Standard deviation of sensor errors.

For the RdF sensors with a 7-point moving average, the average of the errors turned out to be between -2.0% and +5.0% for all ten ramp tests, with three of the last five tests being within a ±1.0% band. However, the standard deviations for the last five

tests are higher, which may be partially due to the greater temperature range tested. The standard deviations in the errors were from 0.8 to 2.0 percentage points, with the majority being less than 1.5.

The Vatell sensors, on the other hand, did not behave nearly as much like one another as the RdF sensors did. As stated in the section on Recalibration & Temperature Correction Tests, the corrections for the Vatell sensors were calculated individually since they behaved differently from one another in later tests. This issue needs further exploration to determine the cause. The errors in the Vatell sensors also tended to be much higher than that for the RdF sensors. (Smoothing does not affect the average errors as the smoothing is only an average itself, but it does slightly improve the standard deviation.) From inspection of the original emissivity data, the Vatell sensors tended to perform worse when the ramps were near the extremes, and better when they were near the middle temperatures and at steady room temperature.

A word should be said about the expected emissivity used for calibration. Since the exact emissivity of paints often depends partly on the uniformity of application (for example, in sample thickness), there may be some differences in the emissivity among samples. Moreover, the optical measurements performed by Sheldahl actually use the normal emissivity to approximate hemispherical emissivity. In fact, the emissivity of Aeroglaze Z306 is quoted by the manufacturer as 0.90, while Sheldahl measured the sample at 0.935. This adds a further uncertainty, due to possible differences in the samples measured. It is difficult to quantify this error, but attempts were made to apply all the samples in the same way.

Chapter 8: Space-Based Experiment

Need for Space-Based Measurements

Several environmental effects can contribute to changes in the properties of thermal control surfaces in space: [8]

- Solar irradiation (ultraviolet rays)
- Contamination
- Charged particles
- Micrometeorite bombardment
- Inherent outgassing products
- Reaction with atomic oxygen
- and probably others.

These effects make it beneficial to study the emissivity and absorptivity of samples in a space environment and over extended periods of time. Characterizing changes in emissivity and absorptivity during and after exposure to the space environment for a material is important to spacecraft design since it affects the continued operation of the thermal control system. Not only can the HFB technique be used to measure the emissivity of surfaces at a single time during their operation in space, but it can also be used to evaluate the coatings over time in the space environment.

Past Space-Based Experiments

Performance of ESR on Space Technology 5 Satellites

The Sensortex ESR was one of two variable emissivity coatings launched on the Space Technology 5 (ST-5) satellites in 2006.[21] Sensortex tested two ESRs, each consisting of 4 separate sections and totaling 57.6 cm^2 of active area, on two satellites.

The ESR devices were tested prior to launch using a calorimetric system. They were placed on a plate at a set temperature and the power required to maintain the plate temperature was measure to quantify heat loss. The change in emissivity ($\Delta\varepsilon$) between "off" and "on" states was then calculated from the heat loss. Activating the ESRs with an applied voltage of 400 V, the two ESRs showed changes of $\Delta\varepsilon = 0.55$ and $\Delta\varepsilon = 0.43$. In space, one ESR showed a $\Delta\varepsilon$ of 0.37 at the beginning of the ST-5 mission, dropping to about 0.33 toward the end of the mission. The other ESR experienced a fault early in the mission and measurements could not be obtained.

The reason for the drop in $\Delta\varepsilon$ from the beginning to the end of the mission was thought to be ionizing radiation which caused the ESR to remain in a "partially on" state (membrane partially sticking to the skin), not returning to the low value when deactivated in subsequent cycles. This problem seems to be reduced by newer generations of Sensortex's membrane material which use conductive black Kapton, as well as by applying a negative polarity high voltage for a short time, which was explained earlier in the section on Membrane Sticking of the ESRs in laboratory tests of the HFB method.

Design of MISSE Module

A module was designed for testing the heat flux-based emissivity measurement technique with both passive and active surfaces as part of the Materials International Space Station

Experiment 6 (MISSE-6). The module had to be made such that it could be bolted to the a platform inside one of two "suitcases" which will hold all the MISSE-6 experiments. Once in space, the suitcases will be attached to the outside of the Space Station and opened out to expose the experiments to the space environment. Data loggers are to be attached to the reverse side of the platform to which the experiments are attached.

The MISSE module for the heat flux-based emissivity measurement system includes an iridited (gold-coated) aluminum housing which holds 4 passive and 2 active surfaces, incorporating the HFB emissivity measurement system to measure the emissivity of the surfaces real-time as they operate in orbit on the outside of the International Space Station (ISS). The four passive surfaces are: Aeroglaze Z306 flat black absorptive polyurethane paint, Aeroglaze A276 glossy white reflective polyurethane paint, Vel-Black, and gold-coated polyimide tape for a low-emissivity reference. The active surfaces are two ESRs made by Sensortex which incorporate heat flux sensors into the structure. All the exposed aluminum parts had to be iridited to protect from oxidation in the space environment.

The MISSE housing, which measures 4.000 in x 6.000 in x 0.875 in (10.16 cm x 15.24 cm x 2.223 cm), holds the electronics necessary for the operation of the active surfaces, including two high voltage amplifiers. The ISS provides a 5 V power supply which will power the amplifier and the rest of the electronics. Data is taken by three data loggers (two Veriteq Spectrum models SP-1700-51N, one SP-4000-411) which are located outside the module and connected by 9-pin D-sub style electrical connectors. Two thermocouples fixed to the inside of the housing (Figure 42) measure the temperature of the module. Two small photodetectors are incorporated into the housing

surface to track when the module “sees” the sun and when it “sees” space/shadow. The data from the photodiodes will be used as a check for the heat flux data.

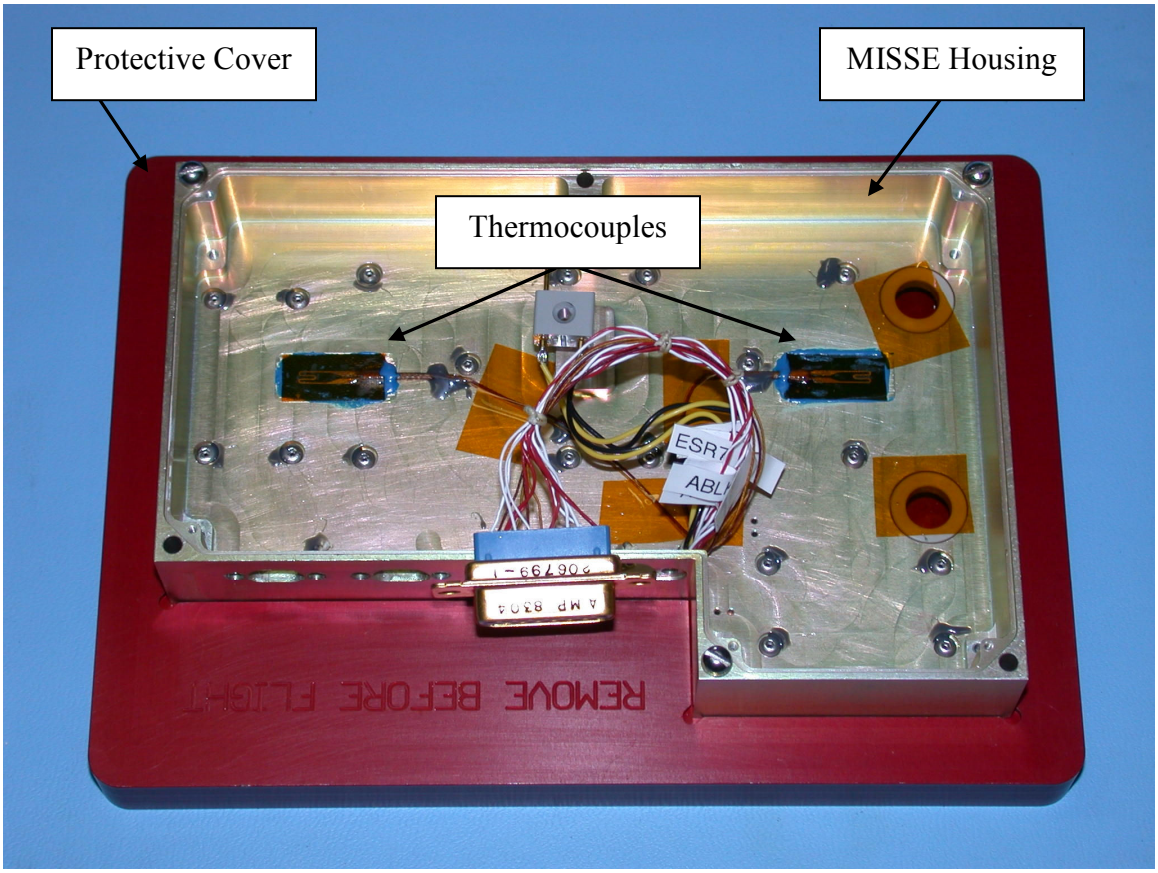

Figure 42. Inside of MISSE module housing showing placement of thermocouples.

The coated heat flux sensors are affixed as units separate from the module housing. Each ESR is mounted to its own iridited aluminum substrate, 2.080 in x 2.080 in x 0.188 in (5.283 cm x 5.283 cm x 0.478 cm) thick, which is attached to the housing from the back by five vented #2-56 x 3/16 in screws. The heat flux sensors for the passive surfaces are mounted two to a substrate onto 2.200 in x 1.100 in x 0.188 in (5.588 cm x 2.794 cm x 0.478 cm) thick iridited aluminum plates. The heat flux sensors used for the passive surfaces on the MISSE module were the Vatell sensors described previously. The coatings were brushed on in the case of the two Aeroglaze paints, while the gold tape was

applied by hand. The Vel-Black assembly was custom made by Energy Science Laboratories inside a thin, iridited aluminum block with a cavity milled out of the center leaving a 0.03 in (0.76 mm) wall thickness. The Vel-Black fibers were deposited in this trough and a parylene coating was applied to prevent fibers from detaching in space which might interfere with other parts of the module and other experiments on the MISSE platform. The Vel-Black casing was then attached to the heat flux sensor by Ablefilm 5025E epoxy. Figure 43 shows the Vel-Black assembly attached to a heat flux sensor next to the gold tape coating on the flight module. Figure 44 shows the face of the module with all the heat flux sensors and coatings attached. The housing contains two circular cutouts for the photodiodes.

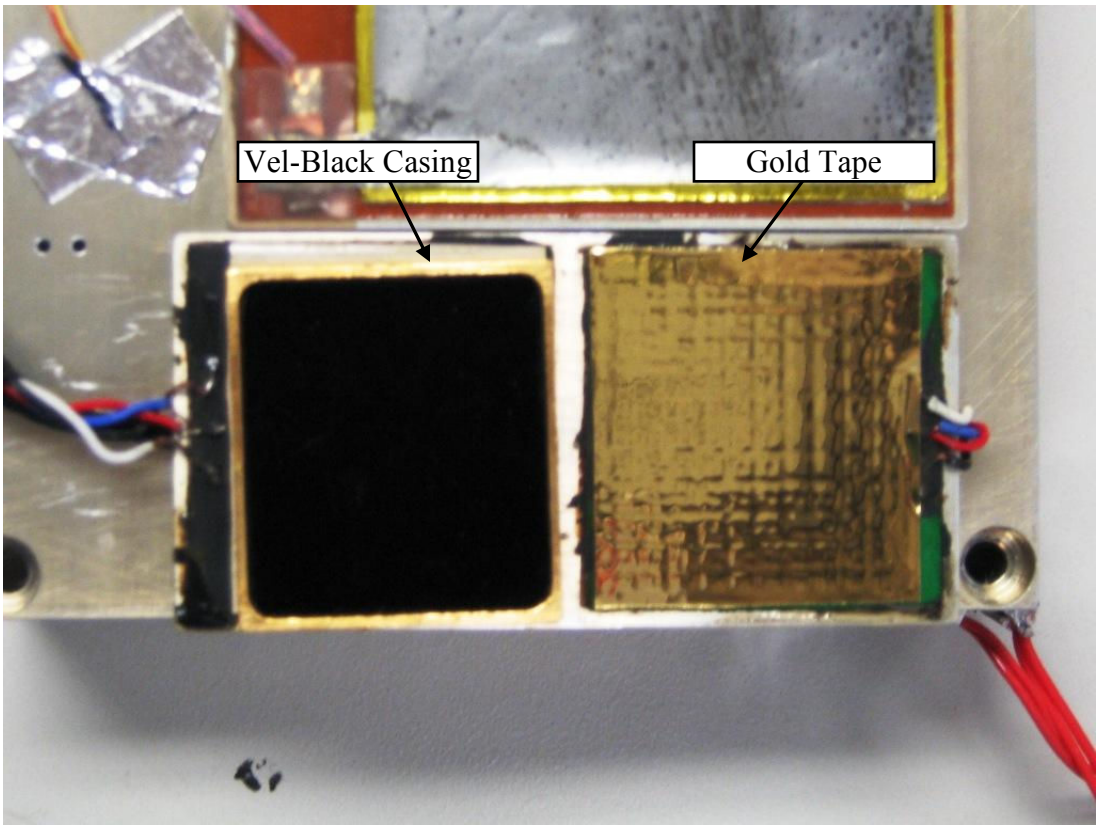

Figure 43. Vel-Black and gold tape affixed to heat flux sensors on the flight module.

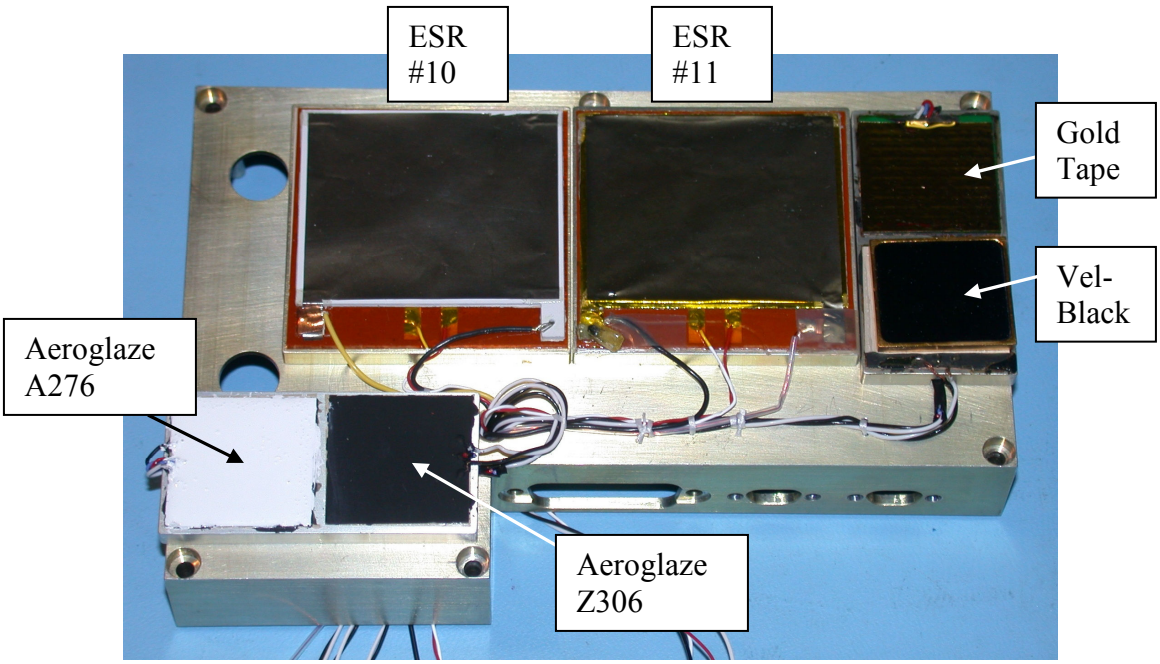

Figure 44. Face of MISSE module with all heat flux sensors and coatings attached.

The MISSE module contains six holes around the perimeter to fasten it to the flight platform by #4-40 x 1 in socket-heat cap screws. These do not have to be vented since the threads in the platform are set in through-holes. All the screws/fasteners used had to be MIL-certified for space flight.

MISSE Module Electronics

The electronics for the MISSE test module (Figure 45) were designed and built by Joe Orndorff of the Johns Hopkins University Instrument Development Group (JHU IDG). The ISS provides 5 V and 15 V inputs which are used to power a timing circuit and voltage amplifiers for the ESRs.

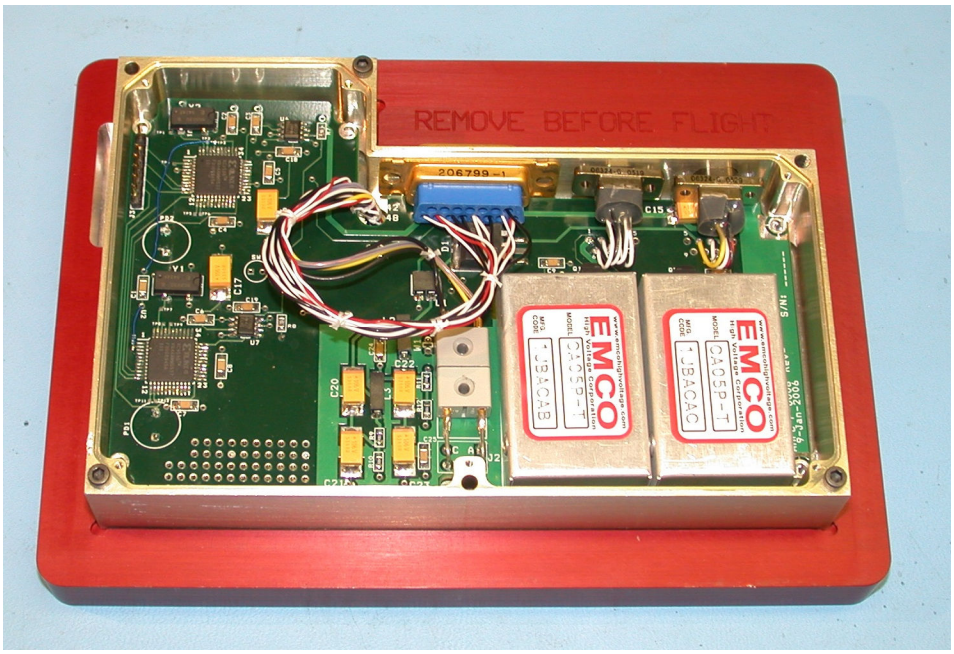

Figure 45. Electronics installed inside MISSE module.

Two high voltage amplifiers were used to amplify the 5V input signal provided by the ship, to actuate the ESRs. The first design incorporated two identical amplifiers (EMCO CA05PT, 0-500Vdc) to allow redundancy in case one failed. However, after finding that a negative voltage applied for a short time helped to de-stick the membrane (apparently by releasing trapped charges in the membrane and/or insulator), one of these amplifiers was replaced with a negative high voltage amplifier. Redundancy had to be abandoned on the amplifier due to the size limitations previously set with NASA.

A timer was incorporated into the circuit to control the actuation time of the ESRs. The actuation was set to turn the ESRs on for 12 hours followed by a negative polarity actuation for 1 minute, then off for 12 hours. This cycle repeats as long as the 5V and 15V inputs from the ship is applied.

The circuit board was screwed into place inside the housing and coated with a clear conformal coating which protects the electronics from outside objects. This is also used to hold all the wires in place, including the heat flux sensor leads, thermocouple

leads, the voltage leads to the ESRs, and the data wires. An aluminum cover screwed onto the back closes off the electronics inside the module housing.

One version of the MISSE module was assembled in August-October 2006 and brought to NASA-Wallops for vibration testing. Figure 46 shows the module on the vibration rig, which subjected the module to random vibrations in all three axes. It passed the tests with no difficulties. A second module was built because of the change in the design of the timing circuit to allow the brief negative polarity actuation of the ESRs for discharging any residual charges, and because the Vatell sensors seemed to perform better than the small RdF sensors. The second and final module was not vibration-tested (though NASA will perform the necessary tests upon integration of the entire MISSE-6 setup) but since the assembly is essentially the same there should be no reason it would fail vibration testing.

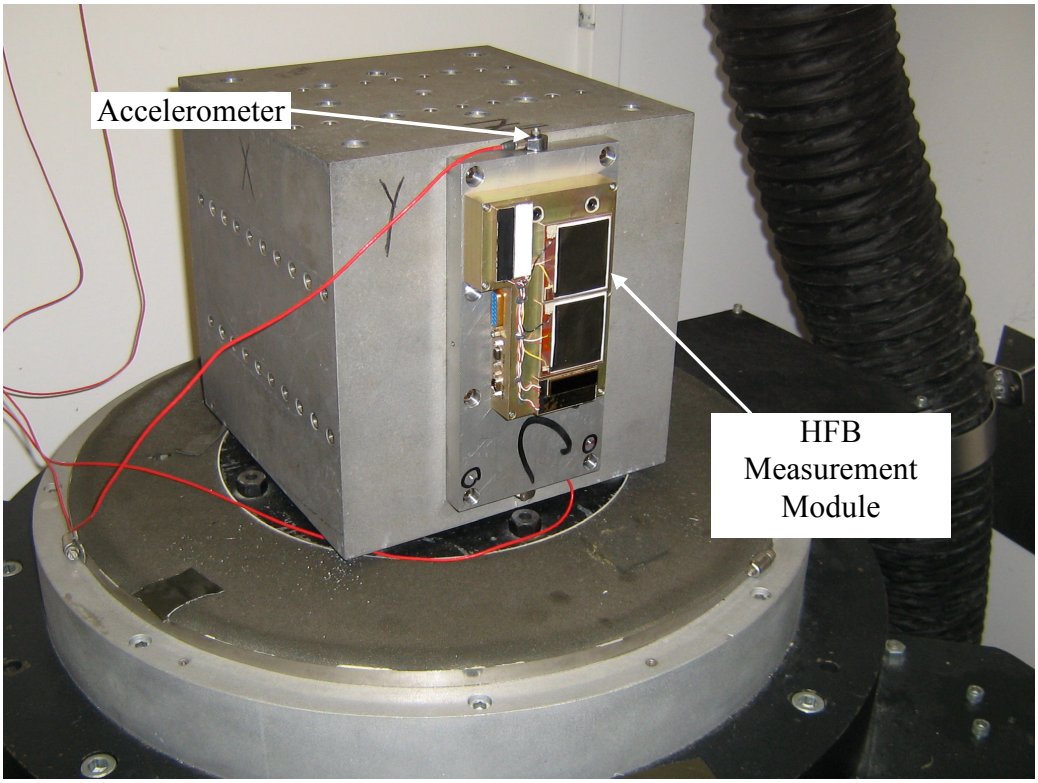

Figure 46. First version of MISSE module on vibration rig at NASA-Wallops.

Data Acquisition on MISSE Module

In order to fully evaluate the heat flux-based emissivity measurement module, the data acquisition required readings from all six heat flux sensors (dual channel DC voltage), the two thermocouples, the two photodiodes, and two lines monitoring the high voltage amplifiers, for a total of twelve data lines. Each of the three Veriteq data loggers has four data input lines, and two also have internal thermocouples for tracking the temperature of the data loggers themselves.

Laboratory Testing of the MISSE Module

Once the heat flux sensors and coatings were attached to the MISSE housing, the module was tested both before and after the electronics were installed. Before installing the electronics in the MISSE module, a series of tests was performed in the vacuum chamber with the same setup as for other tests, except that another copper plate had to be made with two threaded holes to which the MISSE housing could be fastened. The holes were threaded with #4-40 threads as used on the MISSE flight platform, though only two screws were used instead of six. Heaters were placed on three sides of the module housing to control the temperature during tests.

The first test was run at a fairly steady temperature of about 25°C, and the ESRs were activated for about 25 minutes, then deactivated. The emissivity calculation for the passive coatings was performed using corrected calibration values obtained from previous tests with the same sensors coated with Aeroglaze Z306, while the manufacturer's calibration was used for the ESRs. The results are shown in Figure 47 (passive coatings) and Figure 48 (ESRs). The average emissivity measured for the

Aeroglaze Z306 was 0.935, the average for the Aeroglaze A276 was 0.905, for the Vel-Black 0.891, and for the gold tape 0.018.

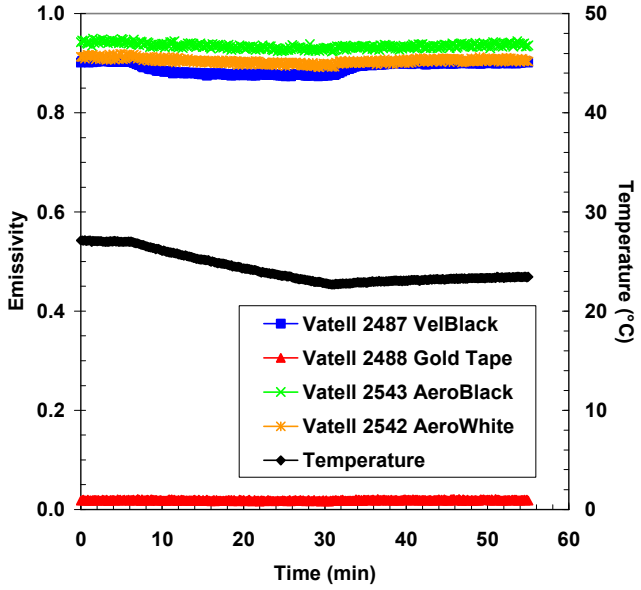

Figure 47. Emissivity measurement of passive coatings on MISSE housing in steady temperature test.

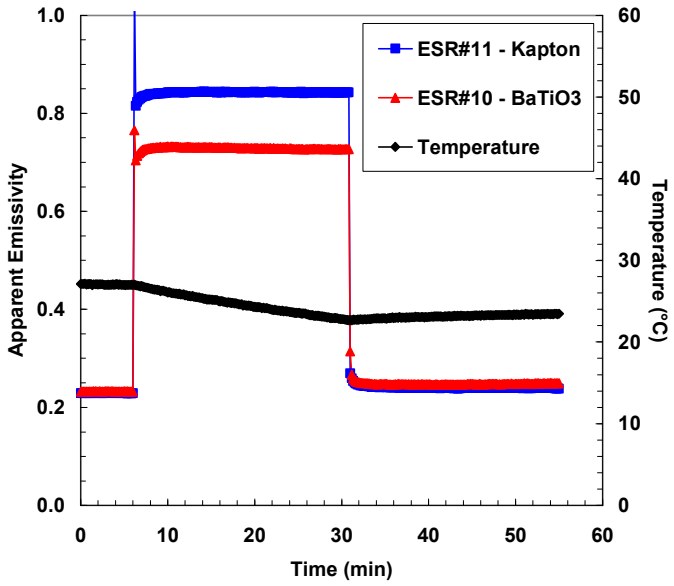

Figure 48. Emissivity measurement of ESRs on MISSE housing in steady temperature test.

After the electronics were installed another set of tests was performed in the vacuum chamber with the entire module and data loggers. This time a steel rod was used to suspend the module from the lid instead of the Teflon rod because of the weight of the module. A rectangular aluminum plate slightly larger than the module was suspended from the rod, and the module was attached to this plate by screws of the same size as are used on the MISSE platform. The three data loggers were held on top of the aluminum plate by two thin metal brackets, and a heater was attached to the underside of each data logger to keep them in their operational temperature range. Wires were connected to the output port of one data logger with feedthrough pins on the other side, so the data logger could be monitored on a computer during the tests. Feedthrough wires were also made for the input power which was delivered by a power supply outside the chamber. An additional two thermocouples were placed on the outside of the module to control and monitor the temperature, and heaters were again placed on three sides of the housing. Figure 49 shows the module in this configuration with all the data, power, and thermocouple wires connected.

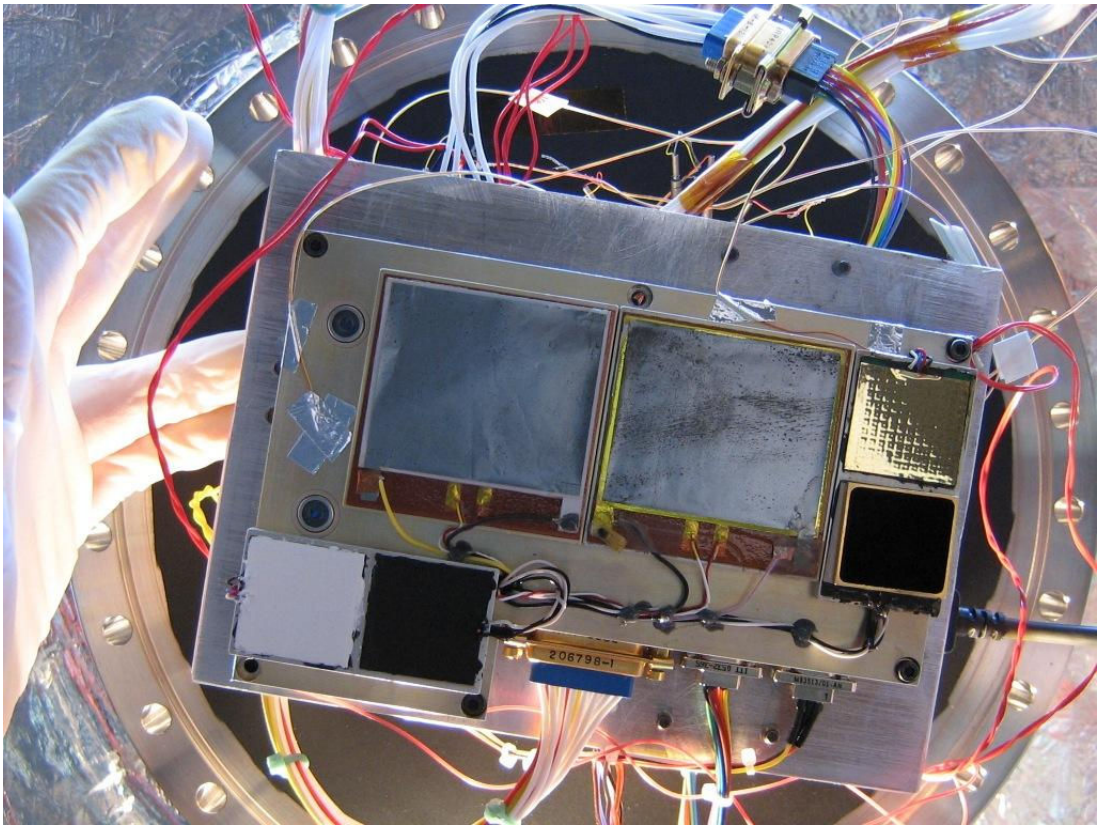

Figure 49. Final MISSE module suspended from vacuum chamber lid before vacuum chamber tests (viewed from below).

A test was performed wherein a temperature controller was programmed to ramp the temperature from 25°C to -25°C, then raise the temperature at a specified rate to -10, 0, 10, 25, and 40°C. This set of tests showed the temperatures of the built-in thermocouples to be consistently higher than the reading from the thermocouple on the outer surface near the photodiodes and the one on the passive substrate near the gold tape-coated sensor, by about 5°C, as shown in Figure 50. Therefore, instead of using the temperature of the two built-in thermocouples, it seemed more fitting to use the temperature of the thermocouple on the passive substrate for the emissivity calculation. However, the data was taken at different rates by the data loggers (reading the built-in thermocouples) and the computer data acquisition (reading the thermocouples on the

outer surface). So instead of trying to match up the temperature and heat flux data for each point in time, the average temperature of the built-in thermocouples was used with an offset of -5°C.

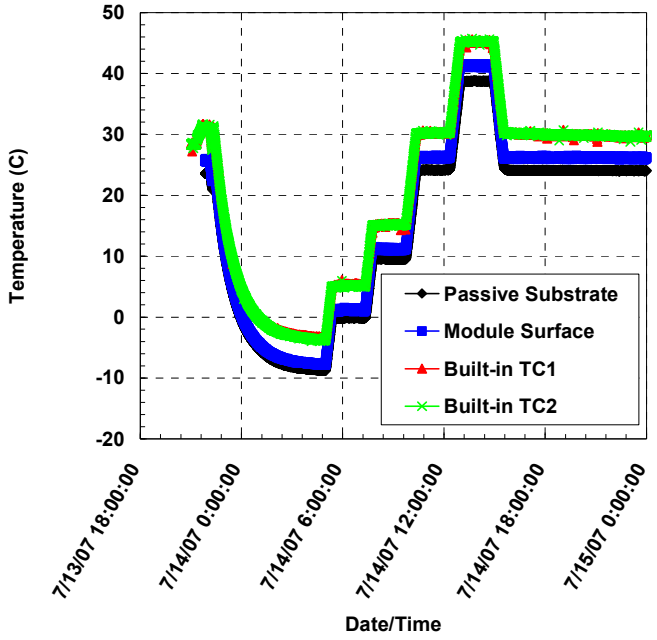

Figure 50. Thermocouple readings on MISSE module during a portion of the vacuum chamber test.

The resulting emissivity calculation for the passive coatings came out steady and close to the expected values as shown in Figure 51. The readings for the three high emissivity coatings were on the low side of the expected 0.935 except when the temperature was at 40°C, with a range of 0.873 to 0.936. Peaks are seen in the Vel-Black emissivity measurement when the temperature was increasing quickly, and valleys when the temperature was dropping, suggesting it took time for the temperature of the Vel-Black casing to adjust when the temperature of the module changed. The emissivity values for the other coatings also curved upwards slightly during the ramp sections of the temperature program, suggesting a similar, though smaller effect with the temperatures of

the other coatings. This behavior appears to scale with the sensor output, as it happened for the gold coating also but is only visible at a much larger scale.

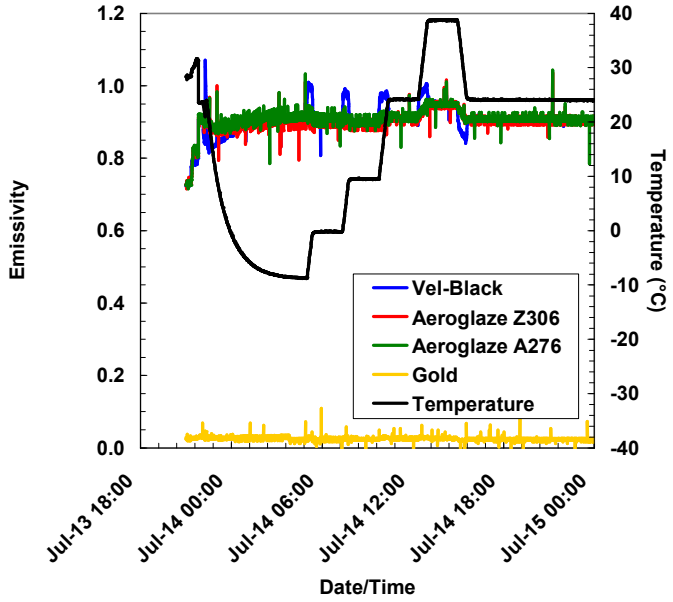

Figure 51. Emissivity measurement of the four passive sensors on complete MISSE module during laboratory tests.

This time, while the sensitivity value for each sensor was used as determined during the previous tests of this set of sensors, the temperature correction used was the quadratic calculated later for the other set of Vatell sensors (explained previously in the section on Recalibration & Temperature Correction Tests). This may indicate that temperature corrections only need to be calculated for a given type of sensor, and not for each individual sensor. This is a positive indication, as it agrees with the manufacturers' method.

The results for ESR#10 are shown in Figure 52. This chart shows three actuations of the ESR. The timing circuit worked without fault, activating the ESR for 12 hours, reversing the voltage for 1 minute, and deactivating for 12 hours. No sticking was seen. The emissivity values were in the expected range, but as with the Vel-Black, peaks were

seen in the emissivity values when the temperature was changing quickly. The emissivity values also curved upwards during the downward temperature ramping.

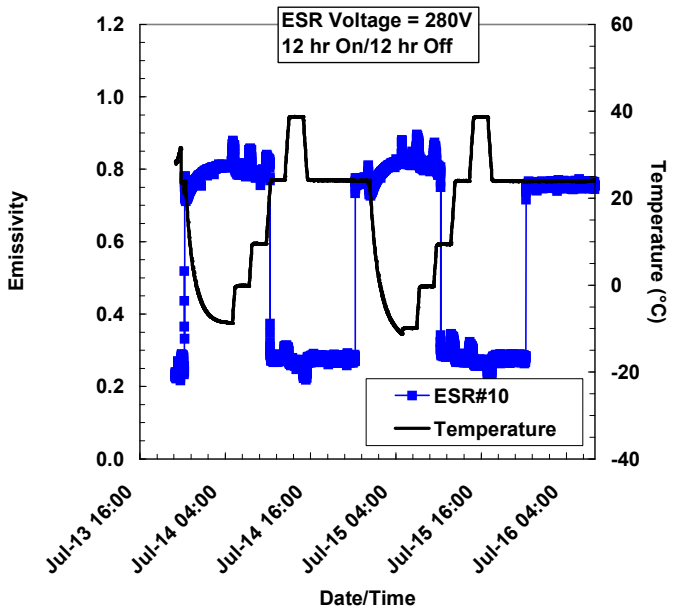

Figure 52. Emissivity measurement of ESR#10 on complete MISSE module during laboratory tests.

Early on in the test after bringing the chamber down to low vacuum, the data line for ESR#11 stopped reading. The data that was obtained was very close to that for ESR#10, so the sensor seemed to be functioning normally. The cause of the disconnection was not discovered though the connector was examined, but the connection problem was fixed after opening the chamber simply by pulling out the connector on the data logger and putting it back in. Unfortunately there was no time to do any more vacuum tests before integrating the module on the MISSE flight platform, so the problem has not been completely identified. However, all the connections will be epoxied in place by the staff at NASA and environmental tests will be performed before flight, and it is hoped that this will reveal any problems that still exist so they can be fixed before flight .

Integration of MISSE Module onto Flight Platform

The HFB measurement module was integrated onto the MISSE flight platform in July 2007 in a cleanroom at the NASA-Langley Research Center. The data loggers were wrapped in MLI and clamped to the back of the platform by custom machined brackets as shown in Figure 53. The HFB emissivity module was then fastened to the front of the platform, and the electrical cables connected as shown in
Figure **54**. Some slack was left in the cables to allow adjustments when other experiments are attached, but once everything is in place the cables will be staked down with a conformal coating epoxy.

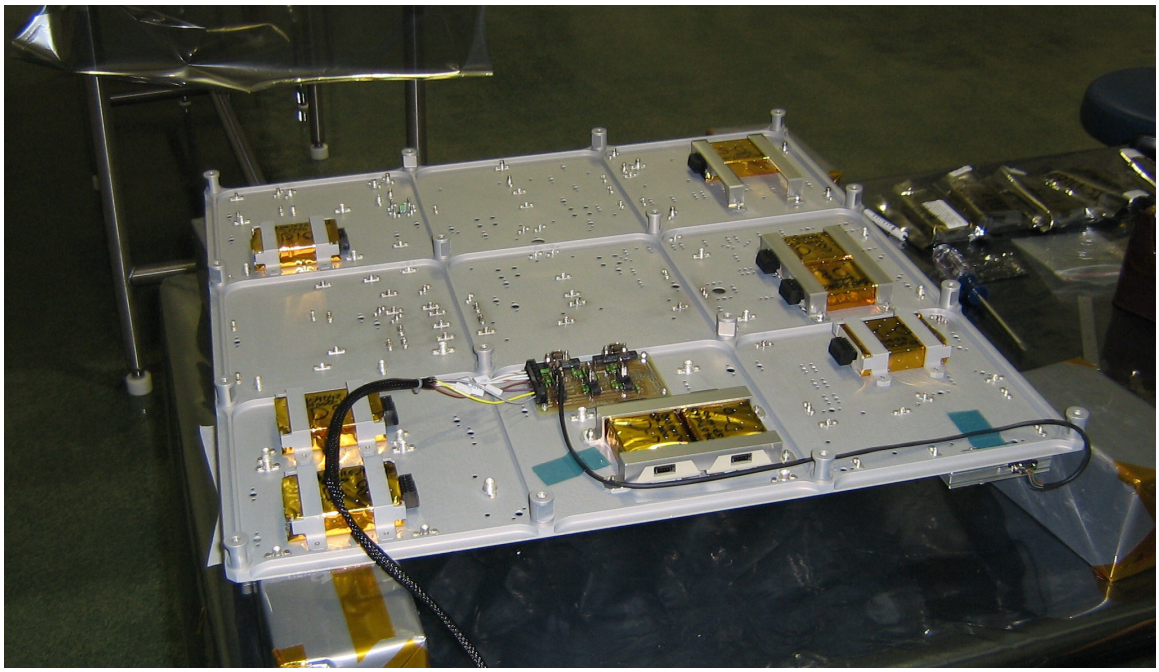

Figure 53. Data logger side of MISSE flight platform. The power supply feed-in can also be seen.

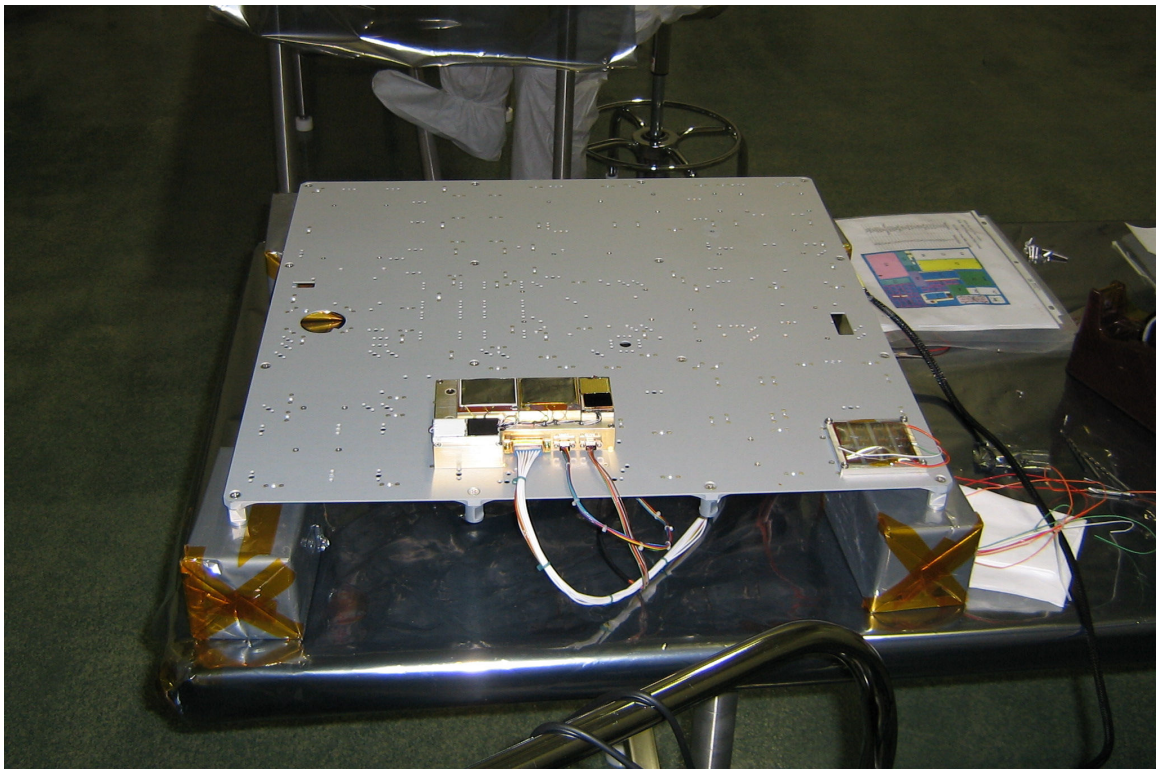

Figure 54. HFB emissivity module on experiment side of MISSE flight platform. Wires have not yet been staked down, and only one other experiment was attached when this photograph was taken.

A power test was performed using a power supply set up for the MISSE platform (Figure 55), which delivered the 5V and 15V signals. The ESRs were seen to activate on turning on the power. The data acquisition lines were also functionally checked by setting the data loggers to start immediately and sample every 10 seconds, while connected to a laptop computer to view the data. The high voltage monitor reading the ESR actuation voltage read the correct value of 2.8 V (corresponding to 280 V applied to the ESRs). All the thermocouple lines read the ambient room temperature. The heat flux sensor lines read values in the correct range and responded appropriately when a light was shined onto them to provide incident radiation.

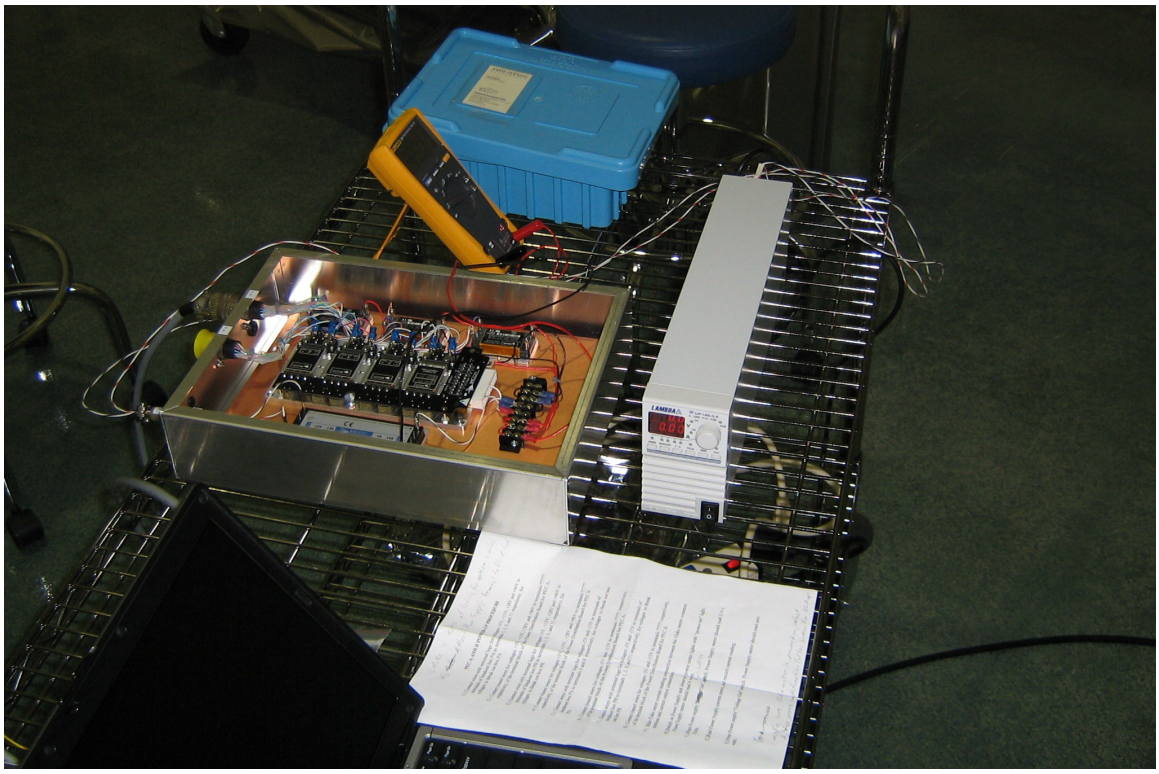

Figure 55. Power electronics used for pre-flight testing of active experiments for MISSE-6.

Environmental testing, including vibration tests, of the entire setup will be performed by the staff at NASA-Langley Research Center. The MISSE-6 experiments are scheduled to be deployed on the ISS in April, 2008. It is hoped that this will further validate the usefulness of the HFB method in determining both absolute emissivity and changes in emissivity for active devices like the ESRs. The high and low known-emissivity surfaces will provide details on the function of the heat flux sensors in measuring emissivity in space over a long period of time. Furthermore, the MISSE-6 experiment will provide another test of the Sensortex ESRs in space, to characterize the behavior of the updated design and provide feedback for improvements that may be made. Most of all, this experiment will help determine whether the HFB emissivity measurement technique is a good candidate for space-based measurement of new

coatings, potentially making better use of data storage and allowing a more compact, simpler setup than an in-space calorimetric measurement.

Chapter 9: Conclusions

A new method has been developed for measuring the emissivity of thermal control coatings by direct measurement of the heat flux through the surface. The heat flux-based technique measures total hemispherical emissivity as in calorimetry, but does not require accounting for parasitic heat losses or knowledge of the temperature history of the sample. It can also be used to measure newly developed active thermal control coatings, including electrostatic devices which cannot be measured directly with optical techniques. Moreover, many active and passive surfaces may be tested on the same substrate simultaneously.

A laboratory experiment has been developed and tested with the HFB technique. The laboratory results show that the HFB technique produces valid measurements over a wide range of temperatures, but more research is needed to completely resolve issues in the calibration and temperature correction of heat flux sensors in the vacuum environment. The method of attaching the sensors is critical, as pressure from air bubbles in the attachment layer significantly affects the heat flux sensor readings. Better calibration of the heat flux sensors in this configuration should make the HFB technique a competitive method of measuring the absolute emissivity of a surface without needing to compare measurements to those obtained by other techniques to obtain accurate results.

The heat flux-based technique may also be useful for absorptivity measurements, with equipment for illuminating the sample in the vacuum chamber. In the space-based measurement, the samples will inevitably operate part of the time in absorbing mode, which will provide knowledge of whether the heat flux sensors react equally when

absorbing, as expected. Future work is recommended to determine any special requirements in application to absorptivity measurements.

A space-based experiment has been designed which is scheduled to deploy on the MISSE-6 mission in April, 2008. If successful, it may be used in the future for measuring the emissivity of thermal control coatings as they function in space, as well as determining the effect of the harsh conditions of the space environment on the coatings.

Appendix A: Parts List for HFB Emissivity Measurement

	Part/Type	Brand	Model
Vacuum Pumps			
Rough Vacuum Pump	Rotary Vane	BOC Edwards	RV8
High Vacuum Pump	Turbomolecular drag pump	Pfeiffer	TMU 065
Turbopump Controller	Electronic Drive Unit	Pfeiffer	TCP015
Pressure Gauge	Compact full range gauge	Balzers	PKR 250
Pressure Readout		Pfeiffer	Pfeiffer SingleGauge
Tubing/Connections			
Turbo to Rough Pump	Steel Flex Hose		KF 16 flex hose 36" long
	Flange clamps		KF16 clamp & center ring
			KF 16 to KF 25 adapter
Chamber to Turbo Pump	Stainless Steel tubing		1/2" OD x 035
	Stainless Steel Compression Tube Fittings	Swagelok	1/2" Swagelok elbows
	Flange to tube adapter	Kurt J. Lesker	1.33" CF Flange to 0.5" tube fitting
Chamber	Basin	Kurt J. Lesker	10.0" OD stainless steel, 8" depth
	Lid (Top Flange)	Kurt J. Lesker	12" CF Flange
	Gasket	Kurt J. Lesker	12.0" Copper Gasket
Liquid Nitrogen Dewar	17.93" ID, 20" OD, 18.0" inner depth Dewar		74.341 lt/hr gross capacity
Feedthroughs			
	Ports on Top (Lid) Flange	Kurt J. Lesker	(5) 1.33" OD ports
Heat Flux Sensor FT	8-pin Power FT 0.032" Copper Conductors	Kurt J. Lesker	1.33" CF Flange
	BeCu Crimp/Solder Connector	Kurt J. Lesker	0.032" dia
Power Feedthrough	10-pin Power FT 0.062" Alumel Conduct.'s		
	BeCu Crimp/Solder Connector	Kurt J. Lesker	0.062" dia
Thermocouple Pins	(2) 5 Pair Type K TC pins	Kurt J. Lesker	(2) 1.33" CF Flanges
Heaters	Kapton Foil Heaters	Minco	Various models
	Power Supply	Staco	Model 3PN221B

Thermocouples	Type K (substrate, wall, lid temperatures)		
	Type T (for LN2 temperature)		
Temperature Controller	Relay output temperature/process control	Love (Dwyer)	26133 (2600 series)
Adhesives	PSA	Minco	Minco #10
	Epoxy-Phenolic	Vishay	M-Bond 600 (bad)
	Epoxy	Emerson & Cuming	Eccobond 285 Black/Catalyst 24 LV
	Film Epoxy	Emerson & Cuming	Ablefilm 5025 E 2-mil (best)
Space-Based Module			
Data logger #1	Universal data logger	Veriteq	Spectrum SP-4000-411
Data loggers #2 and #3	Thermocouple data loggers	Veriteq	Spectrum SP-1700-51N
High Voltage Amplifiers	Positive Amplifier (+500 V)	Emco	CA05PT
	Negative Amplifier (-500 V)	Emco	CA05NT
Electronics/Timing Circuit	Custom design by JHU-IDG		See Appendix B
Logger #1 connector	Microminiature 9 connector		
Loggers #2 and #3 connectors	D-sub 15 connector		
Heat Flux Sensors	Micro-Foil (polyimide)	RdF	27160
		RdF	27142 (Custom 2 in x 2 in)
	Vatell BF	Vatell	BF04
		Vatell	BF07
Data Acquisition	Data Acquisition/Switch Unit	Agilent	34970
	20 Channel Multiplexer/Switch Unit	Agilent	34901A
	Software	Agilent	BenchLink Data Logger Software
	Software for Veriteq Data Loggers	Veriteq	Spectrum Software

Appendix B: Electrical Diagram for MISSE-6 HFB Measurement Module

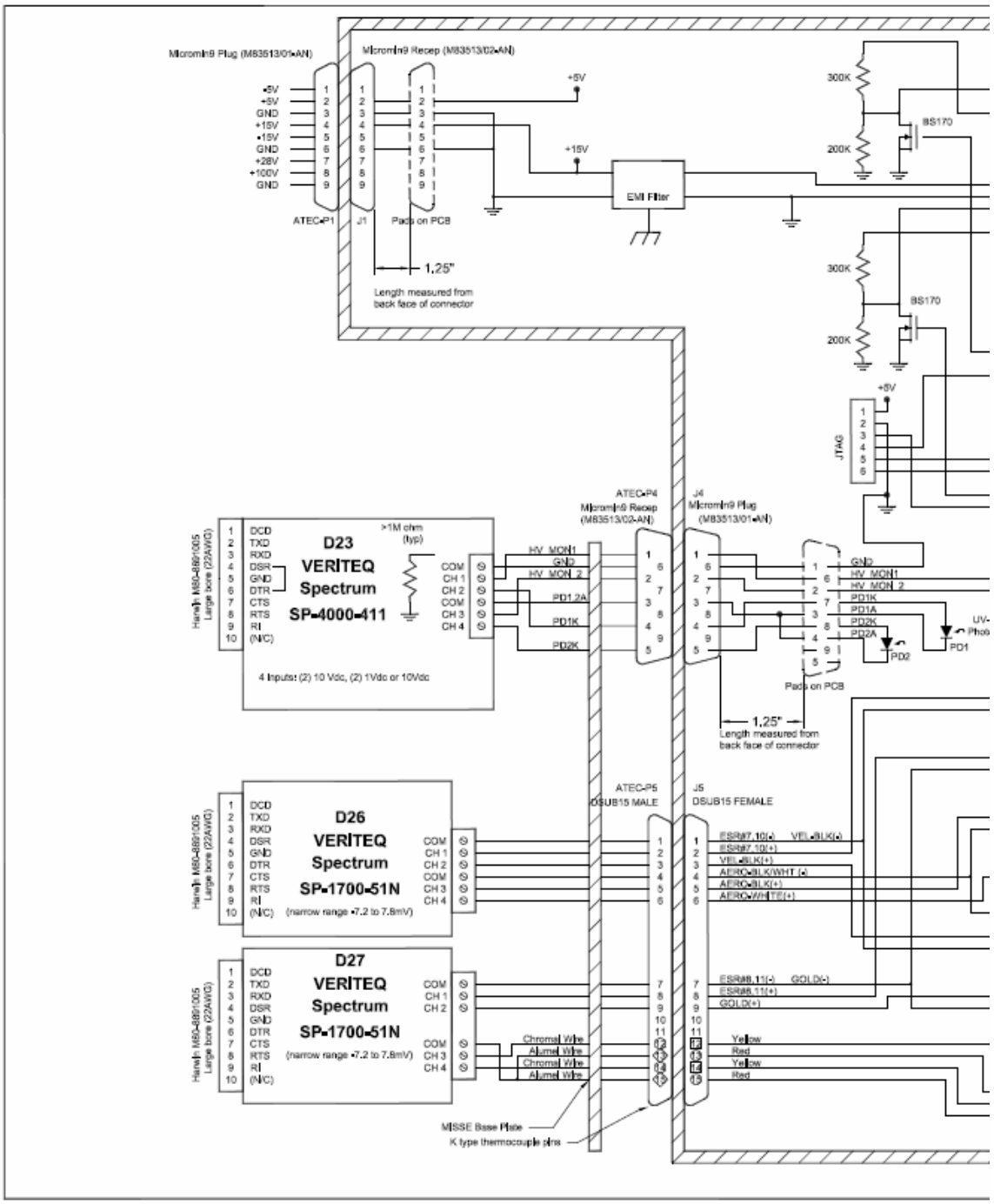

(Continued on next page)

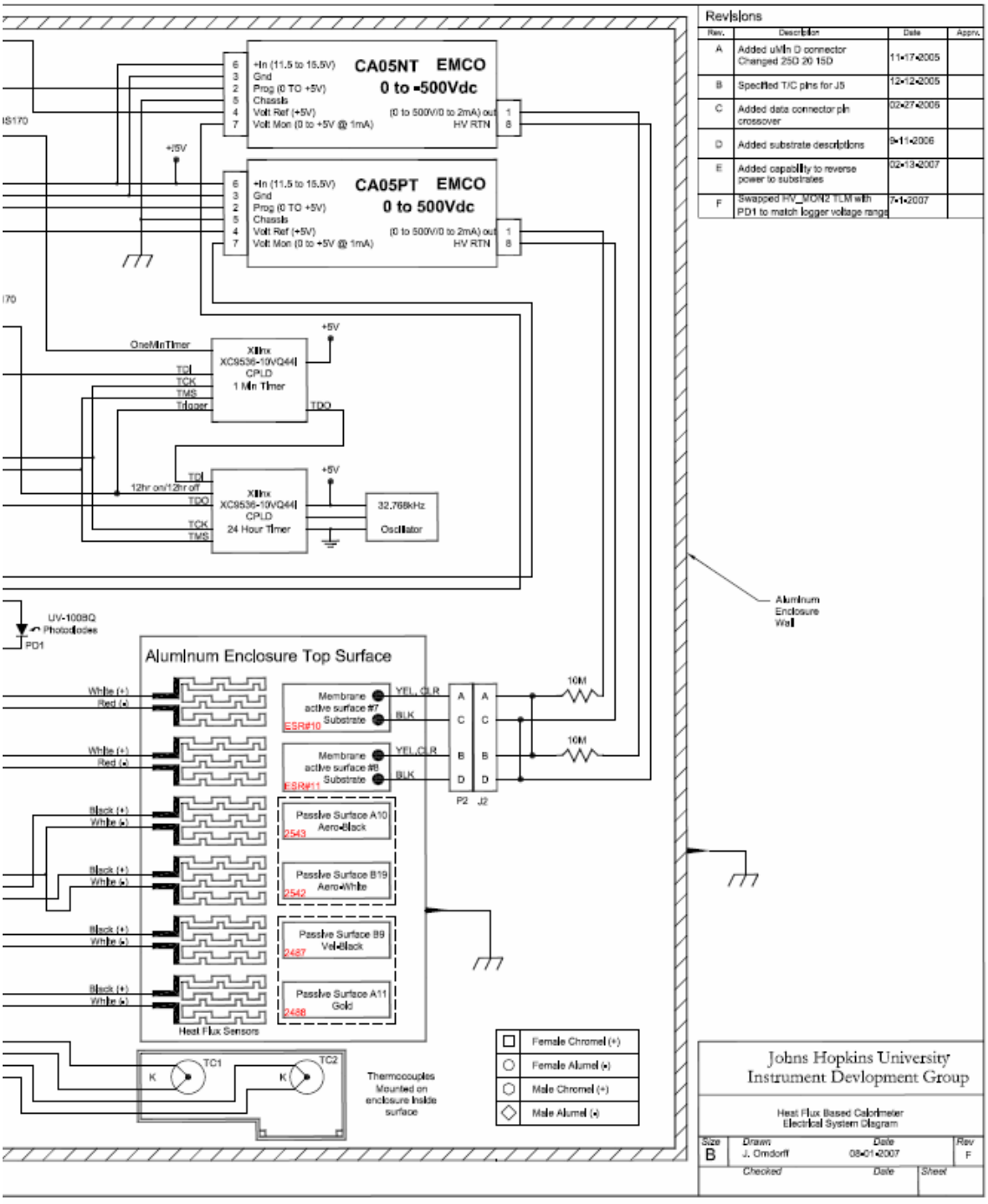

(Continued from previous page)

References

[1] Chandrasekhar, P., et al., "Variable Emittance Materials Based on Conducting Polymers for Spacecraft Thermal Control," *Proceedings of the Space Technology and Applications International Forum (STAIF-2003)*, edited by M. El-Genk, AIP Conference Proceedings 654, American Institute of Physics Press, Melville, NY, 2003, pp. 157-161.

[2] Kislov, N., Groger, H., and Ponnappan, R., "All-Solid-State Electrochromic Variable Emittance Coatings for Thermal Management in Space," *Proceedings of the Space Technology and Applications International Forum (STAIF-2003)*, edited by M. El-Genk, AIP Conference Proceedings 654, American Institute of Physics Press , Melville, NY, 2003, pp. 172-179.

[3] Hale, J.S., and Woollam, J.A., "Prospects for IR Emissivity Control Using Electrochromic Structures," *Thin Solid Films 339*, Elsevier Science S.A., 1999, pp. 174-180.

[4] Biter, W., Oh, S., and Hess, S., "Electrostatic Switched Radiator for Space Based Thermal Control," *Proceedings of the Space Technology and Applications International Forum (STAIF-2002)*, edited by M. El-Genk, AIP Conference Proceedings 608, American Institute of Physics Press , Melville, NY, 2002, pp. 73-80.

[5] Biter, W., Hess, S., and Oh, S., "Electrostatic Appliqué for Spacecraft Temperature Control," *Proceedings of the Space Technology and Applications International Forum (STAIF-2003)*, edited by M. El-Genk, AIP Conference Proceedings 654, American Institute of Physics Press, Melville, NY, 2003, pp. 162-171.

[6] Champion, J.L., Osiander, R., Darrin, M.A.G., and Swanson, T.D., "MEMS Louvers for Thermal Control," *Proceedings of the 2nd International Conference on Integrated*

Micro/Nano Technology for Spacecraft Applications, Los Angeles, CA, 1999, pp. 233-240.

[7] Kauder, L., "Spacecraft thermal control coatings reference," NASA Technical Procedure, NASA/TP-2005-212792, NASA/Goddard Space Flight Center, Greenbelt, MD, July 2005.

[8] Karam, R.D., *Satellite Thermal Control for Systems Engineers*, edited by P. Zarchan, American Institute of Aeronautics and Astronautics, Reston, 1998, pp. 16, 160-164.

[9] Mychkovsky, A., and Ponnappan, R., "Calorimetric Measurement of Emissivity in Space Conditions," *43rd AIAA Aerospace Sciences Meeting and Exhibit*, Reno, NV, January 8-11, 2005, AIAA 2005-961.

[10] Jaworske, D.A., and Skowronski, T.J., "Portable Infrared Reflectometer for Evaluating Emittance," *Proceedings of the Space Technology and Applications International Forum (STAIF-2000)*, edited by M. El-Genk, AIP Conference Proceedings 504, American Institute of Physics Press, New York, 2000, pp. 791-796.

[11] Brosmer, M.A., Fischer, W.D., and Hall, D.F., "Thermal Analysis of Flight Calorimeter Instrument Designs and Calibration Test Methods," *22nd AIAA Thermophysics Conference*, Honolulu, June 8-10, 1987, AIAA 1987-1622.

[12] Scott, R.B., "Heat Transfer by Residual Gas," *Cryogenic Engineering*, D. Van Norstrand, Princeton, New Jersey, 1959, pp. 144-146.

[13] Bohren, C.F., and Albrecht, B.A., "Conductivity of a Gas: A Few Myths Exploded," *Atmospheric Thermodynamics*, Oxford University Press, New York, 1998, pp. 345-346.

[14] Lasance, C.J.M., "The Thermal Conductivity of Air at Reduced Pressures and Length Scales," *Electronics Cooling Online*, Nov. 2002, http://electronics-cooling.com/articles/2002/2002_november_techdata.php, last visited Aug. 10, 2007.

[15] Brewster, M. Q., *Thermal Radiative Transfer and Properties*, John Wiley & Sons, New York, 1992, p. 89.

[16] Holmberg, D.G., and Womeldorf, C.A., "Performance and Modeling of Heat Flux Sensors in Different Environments," *Proceedings of the ASME Heat Transfer Division-1999*, Vol. 364-4, ASME, New York, 1999, pp. 71-77.

[17] Vishay Measurements Group, "Surface Preparation for Strain Gage Bonding," *Instruction Bulletin B-129*, http://www.vishay.com/brands/measurements_group/guide/ib/b129/129index.htm, last visited June 18, 2007.

[18] Farrar, D., Douglas, D.M., Swanson, T., Collins, C., Darrin, A., and Osiander, R., "MEMS Shutters for Thermal Control – Flight Validation and Lessons Learned," *Proceedings of the Space Technology and Applications International Forum (STAIF-2007)*, edited by M. El-Genk, AIP Conference Proceedings 978, American Institute of Physics Press, Melville, NY, 2007, pp. 73-80.

[19] Demiryont, H., and Shannon, K.C. III, "Variable Emittance Electrochromic Devices for Satellite Thermal Control," *Proceedings of the Space Technology and Applications International Forum (STAIF-2007)*, edited by M. El-Genk, AIP Conference Proceedings 978, American Institute of Physics Press, Melville, NY, pp. 51-58.

[20] RdF Corporation, “Simplified heat flow measurement,” http://www.rdfcorp.com/anotes/pa-hfs/pa-hfs_01.shtml, last visited Aug. 7, 2007.

[21] Biter, W., and Oh, S., “Performance Results of the ESR from the Space Technology 5 Satellites,” *Proceedings of the Space Technology and Applications International Forum (STAIF-2007)*, edited by M. El-Genk, AIP Conference Proceedings, American Institute of Physics Press, New York, 2007, pp. 59-65.